Facultad de Ciencias

From Bloch Oscillations to Ohmic Transport

(De oscilaciones de Bloch a transporte óhmico)

Pedro R. López Gómez

Trabajo de Fin de Grado
para acceder al

Grado en Física

Director: Pablo García Fernández

Septiembre - 2019

In all affairs it's a healthy thing now and then to hang a question mark on the things you have long taken for granted.

Bertrand Russell

Agradecimientos

Para la realización de este trabajo ha sido fundamental la ayuda y el apoyo de muchas personas a las cuales me gustaría expresar mi agradecimiento.

En primer lugar, al director de este trabajo, Dr. Pablo García-Fernández, por su dedicación, su atención, y el exquisito trato tanto personal como profesional que he tenido el gusto de recibir durante la realización del mismo, así como por su paciencia e interés a la hora de resolver las numerosas dudas que han ido surgiendo en el proceso.

Al Prof. José Antonio Aramburu, por todos los conocimientos de física del estado sólido que adquirí gracias a sus clases, y por ponerme en contacto con el director de este trabajo. Asimismo, al conjunto de profesores de Física y Matemáticas, por los conocimientos de ambas disciplinas que, con mayor o menor fortuna, han tratado de inculcarme durante estos cinco años.

Me gustaría darle las gracias también a mis once compañeros del Doble Grado, con los que he tenido el placer de compartir estos años de duro trabajo, por su amistad, su ayuda y porque todo este camino habría sido mucho menos agradable sin ellos.

Finalmente, quisiera darle las gracias a mis padres y a mi hermana, por estar siempre a mi lado y por todo lo que hacen por mí, y a Celia, por su cariño, su apoyo y por acompañarme en la tarea de robarle tiempo al hastío y la monotonía.

Abstract

Under the action of an electric field, the electrons in a perfectly periodic ideal crystal do not display a linear acceleration but, instead, present a surprising oscillatory behaviour describing the so-called Bloch oscillations. From the experimental side, early experiments in 1970 by L. Esaki and R. Tsu tried their observation, but it was not until 1992 when J. Feldmann et al. found, for the first time, experimental evidence when working with highly pure semiconductor crystals at very low temperatures. The usual ohmic behaviour arises from the collapse of the perfect periodicity of the crystal due to, e.g. vibrations or impurities, that produces the destruction of these oscillations, making their observation impossible under normal conditions. On the computational side, many simulation methods reproduce the Bloch oscillations; however, few realistic techniques are prepared to simulate their destruction under realistic conditions like finite temperature. Here, we study the evolution of Bloch oscillations into ohmic transport and the various trends with the phonon frequency, the band width and the electron-lattice coupling applying time-dependent second-principles density functional theory on a purely quantum one-dimensional model using the newly implemented scale-up code.

Keywords: Bloch oscillations, transport in solids, ohmic transport, electrical conductivity, electron-lattice coupling, second-principles.

Resumen

Bajo la acción de un campo eléctrico, los electrones de un cristal ideal perfectamente periódico no presentan una aceleración lineal sino un sorprendente comportamiento oscilatorio, describiendo las llamadas oscilaciones de Bloch. Desde el punto de vista experimental, experimentos tempranos llevados a cabo por L. Esaki y R. Tsu trataron de observarlas, pero no fue hasta 1992 cuando J. Feldmann et al. encontraron, por primera vez, evidencias experimentales trabajando con cristales semiconductores de gran pureza a muy bajas temperaturas. El acostumbrado comportamiento óhmico surge debido a las roturas de la periodicidad perfecta del cristal causadas, por ejemplo, por vibraciones o impurezas, que producen la destrucción de estas oscilaciones, lo que hace que sea imposible observarlas en condiciones normales. Desde el punto de vista computacional, numerosos métodos de simulación son capaces de reproducir las oscilaciones de Bloch; no obstante, existen pocas técnicas realistas preparadas para simular su destrucción bajo condiciones realistas como temperatura finita. En este trabajo, estudiamos la evolución desde las oscilaciones de Bloch hasta el transporte óhmico y las diferentes tendencias con la frecuencia de los fonones, el ancho de banda y el acoplamiento electrón-red mediante la aplicación de la teoría del funcional de la densidad de segundos principios dependiente del tiempo, utilizando para ello el código SCALE-UP recientemente implementado.

Palabras clave: Oscilaciones de Bloch, transporte en sólidos, transporte óhmico, conductividad eléctrica, acoplamiento electrón-red, segundos principios.

Contents

CHAPTER 1

Introduction

Transport phenomena constitute a fundamental part of physics and, in particular, they play a key role in solid state physics and chemistry, since their study allows us to know the response of a certain material to perturbations like external fields or temperature gradients [1]. Among these phenomena, electronic transport can be considered as one of the most relevant problems and it has been widely researched and thoroughly characterized through the measurement of the electrical resistivity in almost all materials [2]. However, understanding electronic transport, and in particular electrical conductivity, from a rigorously quantum mechanical point of view is by no means a trivial matter [3], as we shall try to show in the following lines.

Experimentally, it is well known that if we consider a metallic sample and we apply a static electric field $\vec{E}$, it gives rise to an electric current whose intensity is given by Ohm's law [4]:

$$I = \frac{V}{R}\,, \tag{1.1}$$

where V is the potential difference between two points and R is the resistance of the sample, if we assume that the amplitude of the electric field $\vec{E}$ is not so high as to produce a non-ohmic behaviour. This equation is usually expressed in terms of the electric current density $J = I/A$, where A is the transverse area of the sample, as follows [4]:

$$J = \sigma E\,, \tag{1.2}$$

where σ is the electrical conductivity, a characteristic parameter of each metal. In fact, σ is not a scalar but a second order tensor. However, since in this work we shall be dealing with a one-dimensional system, we shall only be concerned with the component of such tensor corresponding to the longitudinal direction of our system.

In accordance with what has been set out in the above paragraph, if we applied a constant electric field to a metal, under normal circumstances and due to a long history of measurements, we would expect to observe a constant electric current. Nevertheless, if we considered the same constant electric field, but now applied to a *perfectly* periodic ideal crystal, according to the quantum equations of motion [5] the electric current would not be, by any means, constant, but it would display a surprising oscillatory behaviour with time, and so Ohm's law would not be applicable. Thus, in such ideal crystal, the electrons do not display a linear acceleration but, instead, they present an oscillatory behaviour, describing the so-called *Bloch oscillations*, named after the Swiss physicist Felix Bloch (1905-1983). Naturally, a great number of questions arises at this point:

- What is the origin of these oscillations?
- Why do not we observe them under normal conditions?
- How does the evolution occur from such oscillations to the ohmic transport that we are accustomed to observing?

One of the main objectives of this work will be trying to answer these questions. There is another crucial issue related to the previous ones, which is the origin of resistivity in solids, a topic that has aroused great interest since the beginning of the twentieth century. Thus, we can mention different and wrong attempts to arrive at the correct explanation of this phenomenon, such as the known one made by the German physicist Paul Drude (1863-1906) in 1900 [6], when he introduced his classical free electron model for metals, or the different speculations which signaled that electrical resistivity was due to the scattering suffered by the electrons when crossing the barriers of the crystalline potential. The true cause of resistivity, however, is the electron-lattice interaction [1], that is, the interaction between an electron, conceived to be in a particular state described by a wave function, and a lattice vibration, described by a phonon eigenstate. The basic idea of this process is quite simple. The phonon disturbs the lattice, displacing some atoms from their reference positions in the crystal. An electron is affected by the change of position, and is thus liable to be deflected, or scattered, out of its accustomed course. For example, a longitudinal vibration compresses or expands the lattice at various points, at which the effective electrostatic potential acting on the electron is changed, and there is the possibility of scattering. In this interactions the total wave vector is conserved, that is, the electron can only be scattered if a phonon is emitted or absorbed and the total wave vector not changed except by a reciprocal lattice vector [1]. In Figure 1.1 we show a very schematic cartoon that might be of help to visualize the difference between Bloch oscillations and ohmic transport.

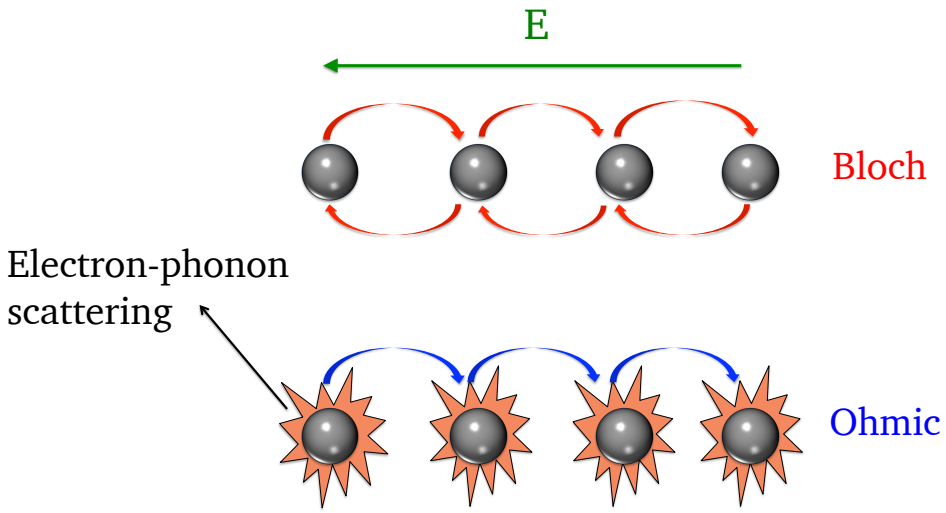

FIGURE 1.1. Schematic cartoon which illustrates the difference between Bloch oscillations and ohmic transport. Upon the application of a constant electric field, the electrons in a perfectly periodic ideal crystal display an oscillatory behaviour. However, the lattice vibrations cause the collapse of the periodicity and, therefore, the scattering of the electrons by phonons, giving rise to an ohmic transport regime in which the electrons are continuously transported against the field.

Experimentally, electrical resistivity has been thoroughly studied and the relationship between it and atomic vibrations is perfectly characterized. In Figure 1.2 we show the experimental results of one of the numerous studies of resistivity in solids carried out, where the linear dependence between the concentration of phonons and the electrical resistivity is clearly appreciated [7].

However, although numerous phenomena involving electron-phonon interactions have been studied in recent decades through first-principles simulations [8], the study of transport phenomena, and electrical conductivity in particular, from a theoretical/computational point of view constitutes an important weak point of Theoretical Solid State Physics, as there are no methods that allow realistic simulations of transport phenomena. Therefore, to study phenomena such as the destruction of Bloch oscillations due to atomic vibrations or the behaviour of the electrical conductivity at room temperature, it will be necessary to resort to other kinds of approaches

such as the second-principle techniques.

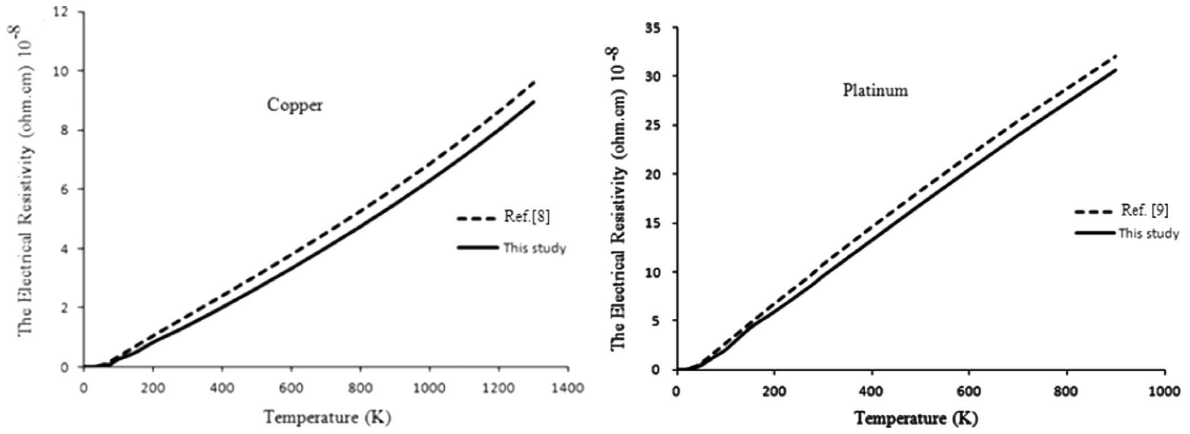

(a) (b)

FIGURE 1.2. Experimental results of the electrical resistivity of copper and platinum as a function of temperature. It is clearly observed that the phononic contribution to electrical resistivity depends linearly on temperature. Both figures were extracted from Ref.[7].

1.1. Objectives of this work

In order to clarify the purpose of this work, it is necessary to specify the principal objectives pursued by this dissertation so that they can serve as a guide for further discussions. Hence, we can distinguish two fundamental objectives:

- On the one hand, we aim to check how Bloch oscillations arise at a temperature $T = 0\,\mathrm{K}$ in a purely quantum model of a one-dimensional tight-binding chain, that is, without taking into account any of the assumptions of the semiclassical transport theory, and to study the role of the electron-lattice interaction in the evolution from these oscillations into ohmic transport when we increase the temperature and, therefore, introduce soft vibrations of the atomic nuclei.
- On the other hand, we want to study the dependence of the electrical conductivity on the different parameters such as the amplitude of the applied electric field, the band width, the phonon frequency or the electron-lattice coupling.

As it has been already mentioned, to achieve these objectives it is necessary to resort to the second-principles techniques, so another objective of this work is to become familiar with this kind of approaches and to understand the theoretical foundations of the first and second-principles methods, as well as their range of validity and their limitations.

1.2. Structure of this essay

Before finishing this brief introduction, it is convenient to give an overview of the structure of this essay. First, in Chapter 2 we shall expose some fundamental concepts of quantum transport theory, with particular emphasis on the origin of resistivity in solids and on the theoretical justification of Bloch oscillations, for which we shall resort to the semiclassical transport theory. After that, in Chapter 3 we shall present the theoretical basis of the computational methods used in this work, with particular reference to first-principles —especially density functional theory— and second-principles methods, with the intention of setting the background where the simulations are carried out. Subsequently, in Chapter 4 we shall show the principal results with a detailed discussion of their most relevant aspects, with a particular emphasis on the

systematic study of the current and the polarization in the case $T = 300\,\mathrm{K}$, in which we shall study the influence that the different parameters of the system have on such magnitudes. Finally, in Chapter 5 the main conclusions of this work will be set out and we shall give an overview of possible extensions of the topic explored in this dissertation.

CHAPTER 2

Fundamentals of Quantum Transport Theory

INTRODUCTION. Before describing the methods used in this work and the results obtained through them, it is convenient to introduce some concepts that will be useful in further discussions and also to make a light review of some notions of solid state theory, in particular concerning quantum transport theory, in order to provide with a theoretical background for the problems and questions which we shall deal with in subsequent chapters. Hence, in this first chapter we shall remember the fundamental Bloch's theorem and the principal resistivity mechanisms in solids, we shall see, theoretically, what happens when an electric field is applied to a periodic system, and we shall tackle the problem of Bloch oscillations within the framework of the semiclassical transport theory.

CONTENTS

2.1. Bloch's theorem and the origin of resistivity in solids

Bloch's theorem is an essential result of solid state theory introduced by F. Bloch in his doctoral thesis (1928) [9] and it is key to properly understand the physics of electrons in a periodic crystal. Although its relevance has been already highlighted during the degree, it is convenient to write it down once again due to its relevance in the discussions that follow. This theorem can be stated as follows [10]:

THEOREM 2.1 (Bloch's theorem). *The eigenstates ψ of the one-electron Hamiltonian $H = -\hbar^2\nabla/2m + V(\vec{r})$, where $V(\vec{r}+\vec{R}) = V(\vec{r})$ for all $\vec{R}$ in a Bravais lattice, can be chosen to have the form a plane wave times a function with the periodicity of the Bravais lattice:*

$$\psi_{j\vec{k}}(\vec{r}) = u_{j\vec{k}}(\vec{r})e^{i\vec{k}\vec{r}}\,, \tag{2.1}$$

where

$$u_{j\vec{k}}(\vec{r}+\vec{R}) = u_{j\vec{k}}(\vec{r})\,, \tag{2.2}$$

for all $\vec{R}$ in the Bravais lattice.

PROOF. Let us denote by $\vec{g}$ the reciprocal lattice vectors. It is well known that the wave functions of the electrons under a periodic potential can be written as follows:

$$\psi_{j\vec{k}}(\vec{r}) = \sum_g c_{\vec{k}-\vec{g}}e^{i(\vec{k}-\vec{g})\vec{r}} = \left(\sum_{\vec{g}} c_{\vec{k}-\vec{g}}e^{-i\vec{g}\vec{r}}\right)e^{i\vec{k}\vec{r}} = u_{j\vec{k}}(\vec{r})e^{i\vec{k}\vec{r}}\,, \tag{2.3}$$

where

$$u_{j\vec{k}}(\vec{r}) = \sum_{\vec{g}} c_{\vec{k}-\vec{g}} e^{-i\vec{g}\vec{r}}\,. \tag{2.4}$$

Let us see that $u_{j\vec{k}}(\vec{r})$ has the periodicity of the direct lattice $\{\vec{R}\}$:

$$u_{j\vec{k}}(\vec{r}+\vec{R}) = \sum_{\vec{g}} c_{\vec{k}-\vec{g}} e^{-i\vec{g}(\vec{r}+\vec{R})} = \sum_{\vec{g}} c_{\vec{k}-\vec{g}} e^{-i\vec{g}\vec{r}} e^{-i\vec{g}\vec{R}} = \sum_{\vec{g}} c_{\vec{k}-\vec{g}} e^{-i\vec{g}\vec{r}} = u_{j\vec{k}}(\vec{r})\,, \tag{2.5}$$

since $e^{-i\vec{g}\vec{R}} = 1$ given that $\vec{g}\vec{R} = 2n\pi,\ n \in \mathbb{Z}$. □

This theorem implies that the wave functions of the electrons of a crystal under a periodic potential, the so-called Bloch waves or Bloch functions, can be expressed as a periodic function $u_{j\vec{k}}(\vec{r})$, which depends on how localized or delocalized the considered electrons are, modulated by the plane wave $e^{i\vec{k}\vec{r}}$. Hence, the Bloch waves $\psi_{j\vec{k}}(\vec{r})$ are delocalized throughout the crystal, but they do not have the periodicity of the direct lattice.

It has been already mentioned that the scattering of the electrons when crossing the barriers of the crystalline potential was not the actual reason for resistivity. In order to justify this statement, let us consider an ideal crystal and an electron of wave vector $\vec{k}$ under the crystalline potential $V(\vec{r})$ introduced in Theorem 2.1. Then, it is easy to see that

$$\psi_{j\vec{k}}(\vec{r}+\vec{R}) = u_k(\vec{r}+\vec{R}) e^{ik(\vec{r}+\vec{R})} = u_{j\vec{k}}(\vec{r}) e^{ik\vec{r}} e^{ik\vec{R}} = \psi_{j\vec{k}}(\vec{r}) e^{ik\vec{R}}\,, \tag{2.6}$$

so for two cells separated by a lattice vector $\vec{R}$, the Bloch functions only differ in a phase factor $e^{i\vec{k}\vec{R}}$, and the wave vector $\vec{k}$ of the electron is conserved.

This implies that, even though the Bloch waves $\psi_{j\vec{k}}(\vec{r})$ do not have the periodicity of the direct lattice, the electron density $|\psi_{j\vec{k}}(\vec{r})|^2$ does have it, since

$$\left|\psi_{j\vec{k}}(\vec{r}+\vec{R})\right|^2 = \left|\psi_{j\vec{k}}(\vec{r})\right|^2 \left|e^{i\vec{k}\vec{r}}\right|^2 = \left|\psi_{j\vec{k}}(\vec{r})\right|^2 \left(\cos^2(\vec{k}\vec{r}) + \sin^2(\vec{k}\vec{r})\right) = \left|\psi_{j\vec{k}}(\vec{r})\right|^2\,. \tag{2.7}$$

From Eq.(2.7) it may be concluded that the electron density remains unchanged when the electrons cross the barriers of the potential $V(\vec{r})$, which in turn implies that there would be no loss of charge density and, therefore, no resistivity.

The previous reasoning allows us to affirm that in a perfectly periodic ideal crystal there would be no resistivity. Therefore, it can be concluded that resistivity must be due to the collapse of the perfect periodicity of the crystal, which gives rise to scattering processes of the electrons that causes them to change their wave vector $\vec{k}$. This collapse of the periodicity, that is inevitably present in real crystals, can be due to different causes; the most relevant are the atomic vibrations, the presence of defects and impurities, the interaction between electrons or the presence of ordered magnetic moments, whose periodicity is frequently different to that of the Bravais lattice. Among these resistivity mechanisms, in this work we are going to focus only on the first and, perhaps, the most relevant one, the atomic vibrations, so it is necessary to spend a few words to talk about them.

It is easy to see that atomic vibrations, that is, the movement of the positive cores around their reference positions, break the perfect translational periodicity of the crystalline potential $V(\vec{r})$, so that Bloch's theorem is no longer valid. During the degree, we have studied the classical dynamics of the atomic vibrations within the framework of the harmonic and the nearest-neighbour approximations, and the quantization of the corresponding results in terms of phonons or quanta of vibration. In order to illustrate the relationship between the temperature and the amplitude of the atomic vibrations, let us remember that within the harmonic approximation the vibrational energy is a parabola as the one sketched in Figure 2.1. Hence, taking into account that the vibrational energy is $E \sim k_B T$, it is clear that higher temperatures imply

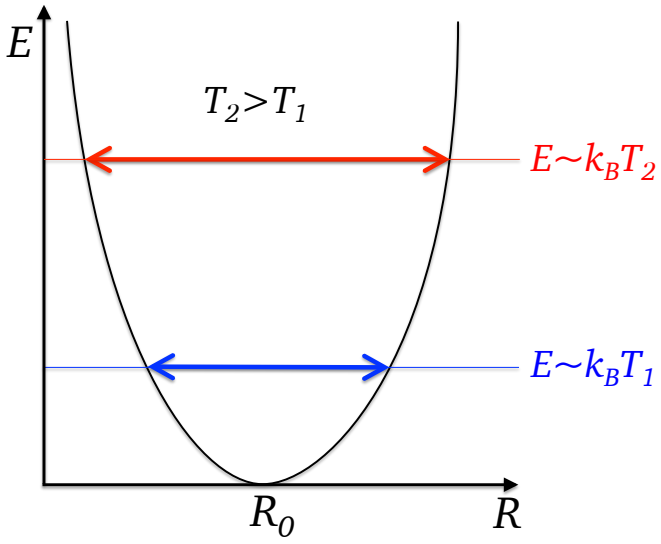

FIGURE 2.1. Schematic cartoon that illustrates the dependence of the amplitude of the atomic vibrations on the temperature.

higher vibrational energies and thus greater amplitudes of the atomic displacements, as it is shown in Figure 2.1.

From the previous paragraph it follows that an increase in the temperature will cause a reduction in the translational periodicity of the crystal, giving rise to more scattering processes of the electrons and thus resulting in a higher electrical resistivity.

The role of temperature and vibrations in the evolution from Bloch oscillations to ohmic transport will be analysed more carefully in Chapter 4 through simulations that will allow us to observe the behaviour of the current and the polarization for different values of the temperature, the phonon frequency and the electron-lattice coupling.

2.2. Electric fields and periodic systems

To properly understand transport phenomena in solids it is necessary to study the dynamics of the electrons under the action of external fields. In this work we shall focus our attention on what occurs when we apply an external electric field to a solid.

In the introduction of this work it was mentioned that when a constant electric field is applied to a perfectly periodic ideal crystal, the electric current presents an oscillatory behaviour, describing Bloch oscillations. In this section we shall justify this statement.

By applying an electric field $\vec{E}$ to the system, the potential energy will be the sum of the crystalline potential $V(\vec{r})$, which has the translational symmetry of the crystal, and the electric potential energy $-e\vec{E}\vec{r}$. This new potential $V(\vec{r})-e\vec{E}\vec{r}$ does not have the translational symmetry of the crystal, as it is sketched in Figure 2.2, but it has the form of a Wannier-Stark ladder [11], which makes extremely difficult to solve the time-dependent Schrödinger equation, whose resolution is essential to study the dynamics of the electrons. Moreover, Bloch's theorem would not be valid either, since one of its hypothesis is that the potential has the periodicity of the Bravais lattice. Nevertheless, it can be proved [12] that introducing a homogeneous electric field produces a displacement of the charge density without changing its spatial periodicity, like a sliding frozen density. Hence, the wave functions of the electrons keep a Bloch-like form but with the difference that they are much more localized that in the absence of electric field.

It must be remarked that developing here a rigorous quantum mechanical treatment of the problem exceeds the scope of this work, so to describe the concepts concerning the dynamics of the electrons of a crystal which are relevant for the present work we shall resort to the

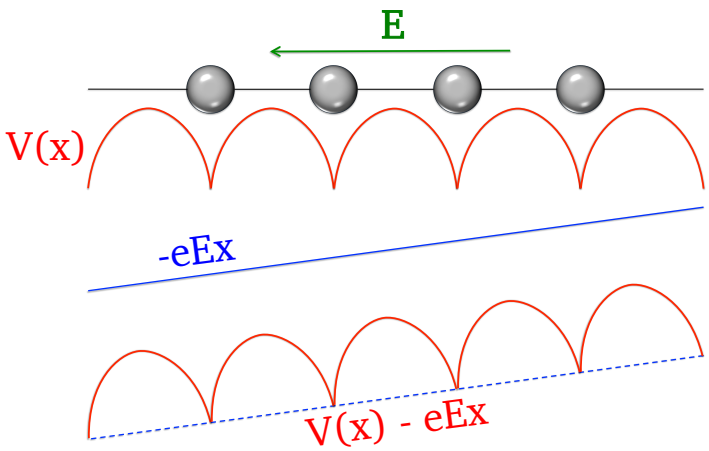

FIGURE 2.2. Schematic cartoon that shows how the introduction of an external electric field breaks the translational symmetry of the crystalline potential. In this case, the electric field pointing to the left causes the energy of the orbitals placed in successive cells to the right to grow in small steps (Wannier-Stark ladder).

semiclassical transport theory, developed by F. Bloch [9] and C. Zener [13]. However, as we shall see in Chapter 3, in this work we shall go beyond these limitations as our computational treatment will be fully quantum mechanical.

2.2.1. The semiclassical transport theory

The semiclassical model considers that electrons keep their quantum nature but that they move under the action of external field according to Newtonian dynamics. In this regard, the delocalized Bloch wave is substituted by a localized wave packet with a wave vector $\vec{k}$ defined up to a reciprocal lattice vector. Hence, this model predicts the temporal evolution, in the absence of collisions, of the average values of the position $\vec{r}$ and the wave vector $\vec{k}$ of the wave packet [10, 14]. For the sake of simplicity, from now on we will denote these average values respectively as $\vec{r}$ and $\vec{k}$ instead of $\langle\vec{r}\rangle$ and $\langle\vec{k}\rangle$. It should be noted that this prediction is based entirely upon a knowledge of the band structure of the metal and upon no other explicit information about the periodic potential of the ions. Thus, the semiclassical model aims to relate the band structure, that is, the form of the dispersion relation $\varepsilon_n(\vec{k})$, where n is the band index, with the transport properties of the metal. Nevertheless, it should be remarked that the validity of this approach is subjected to the following rules [10]:

i) The band index is a constant of motion, so interband transitions are forbidden. Consequently, this approach is valid provided that the external electric and magnetic fields are moderate enough so that the electron cannot jump between bands.

ii) The position and the wave vector of the wave packet evolve according to the classical equations of motion:

$$\frac{d\vec{r}}{dt} = \vec{v}_n(\vec{k}) = \frac{1}{\hbar}\nabla_{\vec{k}}\varepsilon_n(\vec{k})\,, \tag{2.8}$$

$$\hbar\frac{d\vec{k}}{dt} = \vec{F}\,, \tag{2.9}$$

where $\vec{F}$ denotes the external force exerted by external electric and magnetic fields.

Equation (2.9), which relates the variation of $\vec{k}$ with the external force $\vec{F}$, might look similar to the classical equation $\vec{F} = d\vec{p}/dt$, and they are indeed the same in the case of free electrons, for which $\vec{p} = \hbar\vec{k}$, i.e. the total momentum coincides with the crystalline momentum. However, the equality between both equations does not hold when we consider Bloch electrons, since they are

also subjected to the force of the crystalline potential $V(\vec{r})$, which does not change the wave vector $\vec{k}$, and thus there is a term in the total momentum $\vec{p}$ which depends on the crystalline potential.

Since in this work we are interested in the dynamics of electrons under external electric fields, we shall henceforth orient our brief theoretical exposition towards the case in which the external force is exerted by a uniform static electric field. Therefore, first of all we should briefly explain why the semiclassical theory can be applied in that particular case.

As mentioned in the beginning of this section, applying a uniform static electric field pointing to the left causes the energy of the orbitals placed in successive cells to the right to grow in small steps (in the form of a Wannier-Stark ladder), which causes the electrons to no longer tunnel through the wells, but there are reflections and thus interferences between the various waves transmitted and reflected in the wells that make the initial wave packet remain localized, as the semiclassical theory postulates. Moreover, this localization is greater as the electric field is increased. In addition, the localized packets of different bands overlap very little with each other, so that, if the applied fields are not exaggeratedly large, interband transitions are negligible, according to the assumption of the semiclassical theory.

2.2.2. Bloch oscillations

In the previous chapter it has been mentioned that applying a uniform static electric field to a perfectly periodic ideal crystal gives rise to an oscillatory current. Nevertheless, what we observe under normal conditions is that electrons are continuously transported against the field, without a trace of oscillatory behaviour. The justification for this fact is that no real crystal is perfectly periodical, since the resistivity mechanisms already described (atomic vibrations, defects, impurities, etc.) break its translational symmetry, thus causing scattering of the electrons. This scattering occurs, in average, in a time-scale shorter than the period of the Bloch oscillations, making impossible to observe the latter under normal conditions. That period, as we shall see at the end of this chapter, is inversely proportional to the amplitude of the electric field and to the lattice parameter. From the experimental point of view, the first idea to detect them was developed in 1970 by L. Esaki and R. Tsu [15], but it was not until 1992 when J. Feldmann et al. [16] discovered for the first time experimental evidences of Bloch oscillations working with superlattices of highly pure (to minimize the scattering by defects and impurities) semiconductor crystals at very low temperatures (to minimize the scattering by phonons), thereby increasing the relaxation time of the scatterings up to $\tau \sim 10^{-12}\,\mathrm{s}$, and applying very high electric fields $E \sim 10^{8}\,\mathrm{V\,m^{-1}}$ in order to decrease the period of the oscillations up to $T \sim 10^{-14}\,\mathrm{s}$. On the computational side, many simulation methods reproduce the Bloch oscillations. However, few realistic techniques are prepared to simulate their transition under realistic conditions to an ohmic regime under finite temperature, a shortcoming remedied by the second-principles methods that will be discussed in the following chapter.

In this subsection, we shall see how Bloch oscillations arise within the framework of the semiclassical transport theory. According to Eq.(2.9), if a uniform static electric field $\vec{E}$ is applied to a perfectly periodic ideal crystal, we shall have that

$$\hbar\frac{d\vec{k}}{dt} = -e\vec{E} \implies \vec{k}(t) = \frac{-e\vec{E}t}{\hbar}\,, \tag{2.10}$$

where we have integrated the equation and we have taken $\vec{k}(0) = 0$. We see that $\vec{k}(t)$ grows monotonously with t. Thus, the velocity of an electron at time t will be

$$\vec{v}(\vec{k}(t)) = \vec{v}(\frac{-e\vec{E}t}{\hbar})\,. \tag{2.11}$$

Since $\vec{v}(\vec{k})$ is periodic in the reciprocal lattice, the velocity in Eq.(2.11) is a bounded function of time and, when $\vec{E}$ is parallel to a reciprocal lattice vector, oscillatory, which is in striking contrast to the free electron case, where $\vec{v}$ is proportional to $\vec{k}$ and grows linearly in time [10].

Let us think of a simple example in order to illustrate this reasoning. If we consider a one-dimensional tight-binding model, the dispersion relation will have the following form:

$$\varepsilon(k) = -\alpha - 2\gamma\cos(ka)\,, \tag{2.12}$$

and, therefore, the velocity will be given, according to Eq.(2.8), by

$$v(k) = \frac{1}{\hbar}\frac{d\varepsilon}{dk} = \frac{2\gamma a}{\hbar}\sin(ka)\,. \tag{2.13}$$

Taking into account Eq.(2.10), we can also express the velocity as a function of time:

$$v(t) = v(k(t)) = \frac{2\gamma a}{\hbar}\sin(\frac{-eEa}{\hbar}t)\,. \tag{2.14}$$

Figure 2.3 shows schematically the form of $\varepsilon(k)$, $v(k)$, $k(t)$ and $v(t)$ for this case. The velocity is linear in k near the band minimum, like in the case of free electrons, but it reaches a maximum as the zone boundary is approached, and then drops back down, going to zero at the zone edge. Hence, in the region between the maximum of v and the zone edge, the velocity decreases as k increases, so that the acceleration of the electron is opposite to the externally applied electric force [10], something which is completely different from what we are accustomed to observing under normal conditions. When the zone limit $k = \pi/a$ is reached, k cannot grow anymore, since the semiclassical model forbids electrons to change of band, so that the crystalline potential $V(\vec{r})$ causes a Bragg reflection to the state $k' = -\pi/a$. Note that Bragg's law is verified, since $k' - k = -2\pi/a$ is a reciprocal lattice vector. The temporal evolution of k, including the sharp falls due to Bragg's reflections, is also shown in Figure 2.3.

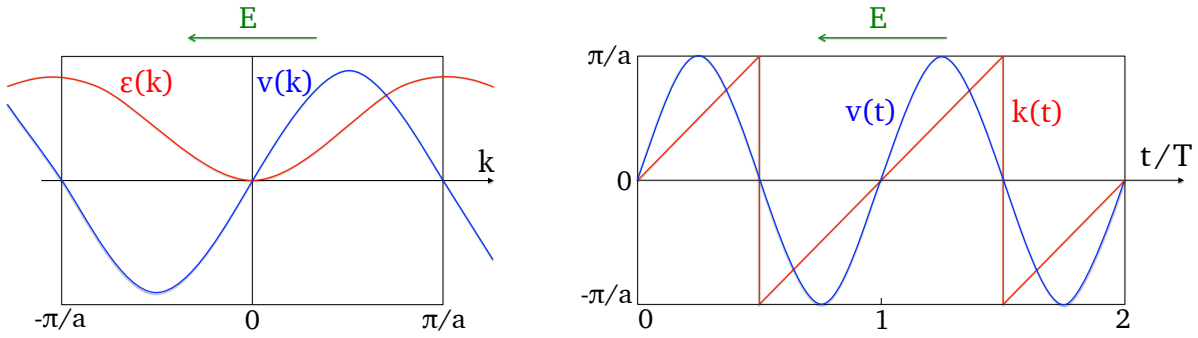

FIGURE 2.3. Schematic cartoon that illustrates the behaviour of $\varepsilon(k)$, $v(k)$, $k(t)$ and $v(t)$ for a one-dimensional tight-binding model when a uniform static electric field is applied. It should be highlighted the oscillatory behaviour of $v(t)$, describing Bloch oscillations.

Therefore, we conclude that if a uniform static electric field is applied to a periodic system, the electrons will describe Bloch oscillations. Moreover, since the electric current is proportional to the velocity of the electrons, it follows that a constant electric field applied to a periodic system will give rise to an oscillatory current, as we shall see through the simulations in Subsection 4.4.1. The period of these oscillations can be easily calculated:

$$k(T/2) = -\frac{eE}{\hbar}\frac{T}{2} = \frac{\pi}{a} \implies T = \frac{2\pi\hbar}{eEa}\,, \tag{2.15}$$

which, for an electric field $E \sim 10^4\,\mathrm{V\,m^{-1}}$, is of the order of $10^{-8}\,\mathrm{s}$.

In this chapter, the theoretical background of this work has been laid down: we have given an overview of some of the fundamentals of quantum transport theory, and the principal phenomena with which this work is concerned, like Bloch oscillations and electrical resistivity, have receieved a little initial discussion. However, as it has been already mentioned, the computational study of these phenomena is very demanding, and thus for its treatment it is necessary to resort to the newly developed second-principles techniques, which are described in detail in the next chapter.

CHAPTER 3

Computational Methods

INTRODUCTION. The development of computational techniques in solid state physics and chemistry has led the theoretical research in these areas to a new level of accuracy and predictive power. Hence, simulations have become a fundamental tool to study the behaviour of molecular and solid-state systems in a cost-effective manner which constitutes an excellent complement to experiments. In this regard, in this chapter we aim to present the theoretical foundations of the principal computational methods used in this work. First of all, an overview of the main first-principles based methods and their limitations will be given, with a particular emphasis on the density functional theory, and especially on the Hohenberg-Kohn theorems and the Kohn-Sham approach. Afterwards, we shall delve into the systematically improvable DFT-based second-principles (SP-DFT) methods, focusing on the reasons which make this approach the best option for our purposes. In particular, the extension of this second-principles approach into the time domain will be introduced as a fundamental tool to study transport properties of solids. Hence, having established the theoretical foundations, the system studied in this work and its different components will be presented and framed within the aforementioned computational methods.

CONTENTS

3.1. Notation

In the following we shall be dealing with a problem of N electrons and M nuclei, and before doing so we shall clarify the notation used in this document.

Regarding the positions, we shall use a capital $\vec{R}$ to denote the positions of the nuclei and a lowercase $\vec{r}$ for the electrons. We shall always label objects related to electrons with Latin alphabet symbols (a, b, $c\ldots$), while those related to nuclei will be labelled with Greek alphabet

symbols (α, β, $\gamma\ldots$). To denote the set of positions of nuclei or electrons we shall use curly brackets, i.e. $\{\vec{R}\} = \vec{R}_\alpha, \vec{R}_\beta, \vec{R}_\gamma\ldots$, and $\{\vec{r}\} = \vec{r}_a, \vec{r}_b, \vec{r}_c\ldots$ Unless necessary, explicit dependencies will be avoided for the sake of readability. When referring to periodic solids, the position of a certain object, like atoms or electronic wave functions, will be given by an index specifying the order in the unit cell and the global Bravais vector of that cell. We shall denote by a bold symbol the set of object and direct lattice vector. For example, $\vec{R}_{\boldsymbol{\lambda}}$ denotes the atom λ of the unit cell at direct lattice vector $\vec{R}_\Lambda$. Henceforth, atomic units will always be used.

3.2. First-principles methods

First of all, we should briefly explain what first-principles or ab initio methods are. In short, these are predictive methods which allow us to solve the Schrödinger equation for N electrons and M nuclei where the only experimental inputs are the fundamental constants, such as the Planck's constant, the mass of the electron, and the atomic numbers of the nuclei [17]. This equation has the following form:

$$\hat{H}(\{\vec{r}\},\{\vec{R}\},t)\Psi(\{\vec{r}\},\{\vec{R}\},t) = i\hbar\frac{\partial}{\partial t}\Psi(\{\vec{r}\},\{\vec{R}\},t)\,. \tag{3.1}$$

Taking into account that the interaction between electrons and nuclei is purely electrostatic (other types of interactions like gravitational or nuclear are negligible), when writing the Hamiltonian we will just consider the kinetic energy of the electrons ($\hat{T}$) and nuclei ($\hat{T}_n$), and the electrostatic interactions between electrons ($\hat{V}_{ee}$), nuclei ($\hat{V}_{nn}$), and electrons and nuclei ($\hat{V}_{en}$) and with external potentials ($\hat{V}_{ext}$). Since in this work we shall not be dealing with time-dependent external fields, we can consider that the Hamiltonian does not depend explicitly on time, and thus the complete, stationary, non-relativistic Hamiltonian can be expressed as follows:

$$\hat{H} = \hat{T}_n(\{\vec{R}\}) + \hat{T}(\{\vec{r}\}) + \hat{V}_{en}(\{\vec{r}\},\{\vec{R}\}) + \hat{V}_{ee}(\{\vec{r}\}) + \hat{V}_{nn}(\{\vec{R}\}) + \hat{V}_{ext}\,. \tag{3.2}$$

The nuclear kinetic energy, considering non-relativistic conditions, can be written as:

$$\hat{T}_n = \sum_\alpha \frac{\nabla_\alpha^2}{2M_\alpha}\,. \tag{3.3}$$

The kinetic energy of the electrons can be similarly defined:

$$\hat{T} = \sum_a \frac{\nabla_a^2}{2}\,. \tag{3.4}$$

Since all the electrostatic interactions have a Coulombic form, we can express the electron-electron and nuclear-nuclear repulsions, as well as the electron-nuclear attraction, in the following way:

$$\hat{V}_{ee} = \sum_{ab} \frac{1}{|\vec{r}_b - \vec{r}_a|}\,, \tag{3.5}$$

$$\hat{V}_{nn} = \sum_{\alpha\beta} \frac{Z_\alpha Z_\beta}{|\vec{R}_\alpha - \vec{R}_\beta|}\,, \tag{3.6}$$

$$\hat{V}_{ne} = -\sum_{a\alpha} \frac{Z_\alpha}{|\vec{r}_a - \vec{R}_\alpha|}\,. \tag{3.7}$$

Hence, we shall define the electronic Hamiltonian as follows:

$$\hat{H}_{el} = \hat{T} + \hat{V}_{ee} + \hat{V}_{ne} + \hat{V}_{nn} + V_{ext}\,, \tag{3.8}$$

which depends only on the nuclei positions but not on their momenta. Furthermore, other operators describing spin-orbit or spin-spin coupling have been also neglected owing to their small contributions for the properties under study [18].

Since the Hamiltonian is time-independent, we can separate the total wave function into a time-dependent part and a spatial part without any loss of generality. Hence, for the A-th stationary state we can write:

$$\Psi_T(\{\vec{r}\},\{\vec{R}\},t) = \Psi_A(\{\vec{r}\},\{\vec{R}\})\Phi_A(t)\,. \tag{3.9}$$

If we substitute this expression on Eq.(3.1), it is clear that we can separate the time-dependent part and the spatial part. Hence, when solving the differential equation, the time-dependent part turns out to be trivial:

$$\Phi_A(t) = \Phi_A^{(0)} e^{-i\omega_A t}\,, \tag{3.10}$$

where $\omega_A = E_A/\hbar$ is the frequency corresponding to the energy E_A of the state. The spatial part, however, depends on both the electron and nuclear coordinates and thus it is much more complex:

$$H\Psi_A(\{\vec{r}\},\{\vec{R}\}) = E_A\Psi_A(\{\vec{r}\},\{\vec{R}\})\,. \tag{3.11}$$

In order to simplify this problem, it is convenient to describe a common approximation that will allow us to decouple the dynamics of electrons and nuclei.

3.2.1. Adiabatic approximation

The expression (3.1) is a second-order differential equation which includes cross terms in Eq.(3.7) that make it impossible to be solved analytically and that is really expensive numerically. For this reason, here we shall consider the adiabatic approximation, which is based, roughly speaking, on the idea that the movement of the nuclei is much slower than the one of the electrons owing to the difference of mass, so that we can consider their dynamics separately [18]. Let us now detail a bit more this approximation. First, note that we can separate the total wave function into electronic, $\tilde{\Psi}_A(\{\vec{r}\},\{\vec{R}\})$, and nuclear, $\Xi_A(\{\vec{R}\})$, wave functions without any loss of generality:

$$\Psi_A(\{\vec{r}\},\{\vec{R}\}) = \tilde{\Psi}_A(\{\vec{r}\},\{\vec{R}\})\cdot\Xi_A(\{\vec{R}\})\,, \tag{3.12}$$

where $\tilde{\Psi}_A(\{\vec{r}\},\{\vec{R}\})$ is chosen so that it is an eigenfunction of the electronic Hamiltonian:

$$H_{el}\Psi_A(\{\vec{r}\},\{\vec{R}\}) = E_A(\{\vec{R}\})\Psi_A(\{\vec{r}\},\{\vec{R}\})\,. \tag{3.13}$$

The equation above is solved, considering the positions of the nuclei not as variables but as parameters, for each possible nuclear geometry. This procedure provides a set of energies $\{E_A(\{\vec{R}\})\}$ which conform an energy surface usually called Adiabatic Potential Energy Surface (APES). Hence, under this approximation we can solve the electronic equation as if the nuclei were frozen to obtain the minimum of $\{E_A(\{\vec{R}\})\}$ and use the corresponding geometry as the one observed in experiments.

The next step is to substitute Eq.(3.12) into Eq.(3.11) and assume that the effect of the nuclear momentum operator on the electronic wave function is negligible, which constitutes a key point of the adiabatic approximation. Under this assumption, and after some calculations, that can be found in detail in Ref.[18], the movement of the nuclei can be obtained from a Schrödinger-like equation under a potential energy which coincides with the aforementioned APES:

$$(\hat{T}_n + E_A(\{\vec{R}\})\cdot\Xi_A(\{\vec{R}\}) = E\cdot\Xi_A(\{\vec{R}\})\,. \tag{3.14}$$

This equation is then solved to obtain the vibrational states and the corresponding vibrational energies, which added to the electronic energies will give us the total energy E of the system. Thus, we have already decoupled the movement of electrons and nuclei as they were independent,

with the total wave function written as a product of the nuclear wave function and the electronic wave function, and a total energy which is the sum of the respective energies.

It should be remarked that under the adiabatic approximation we have considered just one APES, neglecting the coupling between different energy surfaces. However, this is not valid if two or more APES are so close together energetically that the interaction between them cannot be neglected [18].

Once we have introduced these basic concepts, let us focus our attention on two of the most relevant first-principles based methods: the Hartree-Fock method and, especially, the density functional theory (DFT).

3.2.2. Hartree-Fock method

The Hartree-Fock method is historically based on the one-electron approximation made by Hartree and the subsequent corrections made by Slater and Fock in order to force the multielectronic wave function to satisfy the Pauli exclusion principle and the indistinguishability principle. Hence, in the Hartree-Fock approximation, the multielectronic wave function Ψ is considered as an antisymmetrisized product of electronic orbitals, which can be expressed as a Slater determinant in the following form [18]:

$$\Psi(\vec{r}) = \frac{1}{\sqrt{N!}} \begin{vmatrix} \psi_1(\vec{r}_1) & \psi_1(\vec{r}_2) & \cdots & \psi_1(\vec{r}_N) \\ \psi_2(\vec{r}_1) & \psi_2(\vec{r}_2) & \cdots & \psi_2(\vec{r}_N) \\ \vdots & \vdots & \ddots & \vdots \\ \psi_N(\vec{r}_1) & \psi_N(\vec{r}_2) & \cdots & \psi_N(\vec{r}_N) \end{vmatrix} . \tag{3.15}$$

The fact of considering the multielectronic wave function as a single Slater determinant implies that electron correlation is neglected, or equivalently, that the electron-electron repulsion is only included as an average effect [18].

Once the approximated form of the wave function has been introduced, the variational principle is then used to obtain the orbitals that minimize the energy [18]. This procedure leads to the one-electron Hartree-Fock equations:

$$\hat{h}_{HF}\psi_a = \left[\hat{t} + \hat{V}_{ne} + \hat{J} - \hat{K}\right] = \varepsilon_a \psi_a \,, \tag{3.16}$$

where $\hat{J}$ and $\hat{K}$ are one-electron operators and the difference $\hat{J} - \hat{K}$ is the electron-electron interaction. In particular, $\hat{J}$ is the so-called direct interaction term and it stands for the classical repulsion between the electron density clouds:

$$J_{ab} = \int |\psi_a|^2 \, d^3 r_a \int |\psi_b|^2 \, \frac{1}{|\vec{r}_a - \vec{r}_b|} d^3 r_b \,. \tag{3.17}$$

On the other hand, $\hat{K}$ is the exchange interaction, whose origin is purely quantum mechanical and due to the indistinguishability principle:

$$K_{ab} = \int \psi_a^* \psi_b d^3 r_a \int \psi_a^* \psi_b \frac{1}{|\vec{r}_a - \vec{r}_b|} d^3 r_b \,. \tag{3.18}$$

The set of Hartree-Fock coupled equations (3.16) requires the use of computers to obtain its solution, which is found through a self-consistent procedure. Hence, the total energy associated to this method is:

$$E_{HF} = \sum_a \varepsilon_a - \frac{1}{2} \sum_{ab} (J_{ab} - K_{ab}) + V_{nn} \,. \tag{3.19}$$

This energy corresponds to the choice of a single, well-defined configuration, i.e. a single Slater determinant. Nevertheless, the full electronic wave function contains infinite configurations that

are usually approximated as a weighted sum of Slater determinants. The energy associated to the multiple configurations is not, however, the sum of the energy of the configurations, as the interaction among the configurations needs to be considered. The difference between the single configuration energy and the multiconfigurational one is the so-called correlation energy, which is given by:

$$E_c = E - E_{HF}\,, \tag{3.20}$$

where E is the energy associated to the multiconfigurational method. It should be highlighted that multiconfigurational simulations are computationally very expensive and thus they are not adequate for the study of solids, for which it is necessary to consider a different approach.

3.2.3. Density functional theory

As mentioned before, the principal shortcoming of standard ab initio wave function methods like Hartree-Fock is that the wave function Ψ of a N-electron system is typically very complicated as it is a complex-valued function which depends on $3N$ coordinates. In order to overcome these difficulties, in the 1920's, it took place the emergence of an alternative method, in which the energy is not considered as a functional of the wave function but as a functional of the much simpler electron density [18]:

$$n(\vec{r}) = \int |\Psi(\vec{r}, \vec{r_2}, ..., \vec{r_N})|^2 d\vec{r_2}...\vec{r_N}\,, \tag{3.21}$$

which only depends on the three spatial coordinates, no matter how many electrons the system has. This is a significant improvement compared with the previous methods, since the complexity of the wave function depends directly on the number of electrons of the system, but the electron density remains manageable even in large systems. Moreover, the electron density, unlike the wave function, is an observable and, therefore, may be directly related to experimental observation.

Regarding the energy, and considering it as a functional of the density, $E[n]$, it may be divided into three different density functionals: the kinetic energy, $T[n]$; the external potential that does not belong to the electrons, $V_{ext}[n]$; and the electron-electron repulsion, $V_{ee}[n]$, which can in turn be divided into a Coulomb part, $J[n]$, and an exchange part, $K[n]$. The functionals $J[n]$ and $V_{ne}[n]$ are given by their classical expressions [18] :

$$V_{ne}[n] = \sum_{\alpha} \int \frac{Z_\alpha n(\vec{r})}{|\vec{R}_\alpha - \vec{r}|} d^3r\,, \tag{3.22}$$

$$J[n] = \frac{1}{2} \iint \frac{n(\vec{r}) n(\vec{r}')}{|\vec{r} - \vec{r}'|} d^3r d^3r'\,. \tag{3.23}$$

It should be noted that DFT was not really considered as a valuable method until 1964, when Hohenberg and Kohn proved formally their two famous theorems [19], which, combined with the essential Kohn-Sham approach [20], gave rise to a considerable growth of the so-called modern density functional theory.

3.2.3.1. Hohenberg-Kohn theorems

Let us now discuss the two theorems that constitute the basis of DFT. Basically, they express:

i) the biunivocal correspondence between the electron density and the energy of the system and

ii) the relationship between the energy as a functional of the density and the exact energy of the real system.

THEOREM 3.1 (First Hohenberg-Kohn theorem). *For the ground state of any system, the external potential $v_{ext}(\vec{r})$ is determined, within a trivial additive constant, by the electron density $n(\vec{r})$.*

This first theorem has a trivial reciprocal:

COROLLARY 3.2 (Reciprocal of Theorem 3.1). *The electron density $n(\vec{r})$ of the ground state is uniquely defined by the external potential $v(\vec{r})$.*

Considering these two results it is clear that, from the electron density, we can obtain all we need to completely determine the Hamiltonian and, therefore, all the properties of the system. However, the exact functional dependence of the energy on the electron density is not specified by these theorems, which only prove its existence. But we know how the electron density interacts with an external potential, so we can write [19]:

$$E[n] = F_{HK}[n] + \int n(\vec{r})v(\vec{r})d\vec{r}, \tag{3.24}$$

where $F[n]$ is a universal functional valid for any number of particles and any external potential, containing the kinetic energy and the electron-electron interaction.

The second Hohenberg-Kohn theorem is equivalent to the variational principle for electron densities:

THEOREM 3.3 (Second Hohenberg-Kohn theorem). *For a trial ground state density $\tilde{n}(\vec{r})$ such that $\tilde{n}(\vec{r}) > 0$ and $\int \tilde{n}(\vec{r})d\vec{r} = N$, $E_{exact} \leq E_v[\tilde{n}(\vec{r})]$, where $E_v[\tilde{n}(\vec{r})]$ is a trial energy functional for E corresponding to an external potential $v(\vec{r})$ and E_{exact} is the exact ground state solution of the Schrödinger equation.*

Even though these theorems are only stated for the ground state, it has been proved that DFT is also valid for the lower state of any symmetry. Furthermore, considering the Runge and Gross [21] theorems for time-dependent density functional theory (TD-DFT) [22, 23], it has been shown that it can also be applied to excited states.

By the time these two theorems were proved, the main inconvenient was to accurately calculate the kinetic energy, and it was not until 1965 that Kohn and Sham devised a solution to this problem [20].

3.2.3.2. KOHN-SHAM APPROACH

The groundbreaking idea from Kohn and Sham was to substitute the real system of N interacting electrons by a fictitious system of non-interacting electrons, but with the same density as the original one. Since the form of the kinetic energy of a non-interacting system is well-known, the problem now is whether the difference between $T[n]$ and T_S is sufficiently small or not. Thus, let us now delve into the Kohn-Sham method to obtain the exact equation for the energy. In this scheme, they start expressing the universal functional in Eq.(3.25) containing $T[n]$ and $V_{ee}[n]$ as:

$$F_{HK} = T_S + J[n] + E_{xc}[n]\,, \tag{3.25}$$

where $E_{xc}[n]$ is the exchange-correlation functional, which contains all non-classical electron-electron interactions [17]. It is defined as:

$$E_{xc}[n] = T[n] - T_S + V_{ee}[n] - J[n]\,. \tag{3.26}$$

Substituting Eq.(3.26) into Eq.(3.24), we obtain the following expression for the energy:

$$E = T_S + J[n] + E_{xc}[n] + \int n(\vec{r})v(\vec{r})d\vec{r}. \tag{3.27}$$

The only unknown term in Eq.(3.27) is the $E_{xc}[n]$ functional. Thanks to Hohenberg and Kohn theorems, we know that it must be a functional of the electron density, but nothing is known about its exact analytical form and thus we have to use approximations to calculate it.

Since the electron density of the fictitious system S is, by hypothesis, the same as the one of the real system, we can express the exact ground state electron density as [17]:

$$n[\vec{r}] = \sum_j o_{j\vec{k}} |\psi_{j\vec{k}}(\vec{r})|^2 \,, \tag{3.28}$$

where the sum runs over all the so-called Kohn-Sham (KS) orbitals $|\psi_{j\vec{k}}\rangle$ and we have considered that, within periodic boundary conditions, these orbitals can be written as Bloch states characterized by the wave vector $\vec{k}$ and the band index j, with the occupation of a state given by $o_{j\vec{k}}$ [24]. These states are obtained by solving the one-particle Kohn-Sham equations [20]:

$$\hat{h}_0 \, |\psi_{j\vec{k}}\rangle = \varepsilon_i \, |\psi_{j\vec{k}}\rangle \ , \tag{3.29}$$

which are derived by applying the variational principle to $E[n]$ using as the trial electron density the one in Eq.(3.28). In Eq.(3.29), $\hat{h}_0$ is the Kohn-Sham one-electron Hamiltonian, which can be expressed as:

$$\hat{h}_0 = \hat{t} + v_{\mathit{eff}} \,, \tag{3.30}$$

where $\hat{t}$ is the one-particle kinetic energy operator:

$$\hat{t} = -\frac{1}{2}\nabla^2 \,, \tag{3.31}$$

and the term v_{eff} expresses that we can substitute the movement of the real interacting electrons by the movement of the non-interacting ones under an effective potential which has the following form:

$$v_{\mathit{eff}} = v_{\mathit{ext}} - v_H(n;\vec{r}) + v_{xc}[n;\vec{r}] \,, \tag{3.32}$$

where $v_H(n;\vec{r})$ is the Hartree potential:

$$v_H(n;\vec{r}) = \frac{\delta J[n]}{\delta n(\vec{r})} = -\int \frac{n(\vec{r}\,')}{|\vec{r}-\vec{r}\,'|} d^3r' \,, \tag{3.33}$$

and $v_{xc}[n;\vec{r}]$ is the exchange-correlation potential:

$$v_{xc} = \frac{\delta E_{xc}[n]}{\delta n(\vec{r})} \,. \tag{3.34}$$

Therefore, the total DFT energy can be written as [24]:

$$E_{\mathrm{DFT}} = \sum_{j\vec{k}} o_{j\vec{k}} \, \langle \psi_{j\vec{k}} | \, \hat{t} + v_{\mathit{ext}} \, |\psi_{j\vec{k}}\rangle + \frac{1}{2} \iint \frac{n(\vec{r})n(\vec{r}\,')}{|\vec{r}-\vec{r}\,'|} d^3r d^3r' + E_{xc}[n] + E_{nn} \,, \tag{3.35}$$

where the first term on the right-hand side gathers the kinetic energy T_S of the non-interacting system and the action of an external potential.

Apart from the unknown $E_{xc}[n]$ functional, this procedure has also certain limitations and disadvantages, most of them related to the interpretation of the orbitals in Eq.(3.29), since these orbitals are not wave functions corresponding to the real system but to the fictitious one.

Summing up, the main goal of DFT methods is to design $E_{xc}[n]$ functionals increasingly accurate in order to determine the energy of the system as exactly as possible. For this purpose, several methods based on different approximations for the exchange-correlation functional have been devised. Some examples are the Local Density Approximation (LDA) or the Generalized Gradient Approximation (GGA) [25].

There are many other first-principles schemes, and all of them have been a very useful tool during the last decades because of their predictive capacity when applied on simple systems. However, as it has been already mentioned, they present several limitations for the study of large systems with a great number of atoms. In this regard, it should be noted that here we aim to study, among other things, different aspects related to conductivity in solids, a property that cannot be properly understood if we consider just a few hundred of atoms. This is the reason why it is necessary to introduce the so-called second-principles methods.

3.3. Second-principles density functional theory

The study of systems with a large number of atoms, e.g. a simple solid, or which are simulated under conditions like finite temperature or time-dependent external fields, are questions that go beyond the scope of the most efficient DFT schemes, and thus these first-principles approaches are not adequate to our purposes. In order to overcome these limitations, in the last few decades several attempts to tackle this kind of problems have been conducted. Among them, we highlight the self-consistent charge density functional tight-binding (SCC-DFTB) and the effective Hamiltonians or first-principles model potentials. However, these schemes are limited in many aspects, e.g. in the simultaneous treatment of electron and lattice degrees of freedom or when the key interactions involve minute energy differences. In this regard, here we shall focus our attention on the second-principles density functional theory (SP-DFT), a recently developed method that overcomes the mentioned limitations, but which is restricted to problems in which it is possible to identify an underlying lattice or bonding topology that is not broken during the course of the simulation. Nevertheless, this fixed-topology hypothesis is not as constraining as it might seem and permits a drastic simplification of the problem, resulting in a scheme whose accuracy can be systematically improved up to the one of a DFT calculation in the asymptotic limit at a very modest computational cost. Unless otherwise stated, the reference followed in this section will be Ref.[24].

3.3.1. Basic concepts

First of all, it is convenient to mention that one of the key aspects that make SP-DFT so computationally efficient is the use of a basis of localized orbitals formed by Wannier-like functions (WFs henceforth), denoted by $|\chi_{\boldsymbol{a}}\rangle$. Moreover, such functions can be chosen to be orthogonal, of which we shall take advantage in Section 3.5 when calculating the overlap integral in the tight-binding model. This Wannier functions are geometry-dependent, and they are related to Bloch states $|\psi_{j\vec{k}}\rangle$ by unitary transformations. A more detailed description of the relation between both basis can be found in Ref.[24]. Having clarified this aspect, we can go into the foundations of this scheme.

The SP-DFT approach is a first-principles-based method that rests upon a predictive quantum-mechanical theory such as DFT, and it basically relies on two key concepts:

i) The definition of a *reference atomic geometry* (RAG), understood as a particular configuration of the nuclei which is used to describe any other configuration. This RAG is typically chosen to be the ground state structure or any other highly-symmetrical configuration, since these cases correspond to a minimum of the PES and thus all the forces on the atoms and stresses on the cell are zero, which reduces the number of parameters needed and, consequently, the computational cost. Furthermore, the definition of a RAG allows us to specify any possible crystal configuration by expressing the atomic positions as a distortion of the RAG. Hence, with the notation specified in Section 3.1, the position of a particular atom $\boldsymbol{\lambda}$ can be expressed as:

$$\vec{r}_{\boldsymbol{\lambda}} = (\mathbb{1} + \overleftrightarrow{\eta})(\vec{R}_{\lambda} + \vec{\tau}_{\lambda}) + \vec{u}_{\boldsymbol{\lambda}}\,, \tag{3.36}$$

where $\mathbb{1}$ is the identity matrix, $\overleftrightarrow{\eta}$ is the homogeneous strain tensor, $\vec{\tau}_{\lambda}$ is the reference position of atom λ and $\vec{u}_{\boldsymbol{\lambda}}$ is the absolute displacement of atom λ in cell Λ with respect to the strained reference structure.

ii) The division of the actual electron density into a *reference electron density* (RED), $n_0(\vec{r})$, defined for each possible atomic configuration, and a small *deformation density*, $\delta n(\vec{r})$, which acts as a slight perturbation to $n_0(\vec{r})$. Hence, in the SP-DFT approach the electron

density is expressed as:

$$n(\vec{r}) = n_0(\vec{r}) + \delta n(\vec{r}) \iff \sum_{\boldsymbol{ab}} d_{\boldsymbol{ab}} \chi_{\boldsymbol{a}}(\vec{r}) \chi_{\boldsymbol{b}}(\vec{r}) = \sum_{\boldsymbol{ab}} d^{(0)}_{\boldsymbol{ab}} \chi_{\boldsymbol{a}}(\vec{r}) \chi_{\boldsymbol{b}}(\vec{r}) + \sum_{\boldsymbol{ab}} D_{\boldsymbol{ab}} \chi_{\boldsymbol{a}}(\vec{r}) \chi_{\boldsymbol{b}}(\vec{r}) \,, \tag{3.37}$$

where we have expressed the relation also in the WFs basis. In this expression, $d_{\boldsymbol{ab}}$ is the so-called *occupation matrix* for the WFs and we introduce $D_{\boldsymbol{ab}}$ as a *deformation occupation matrix*. In non-magnetic cases, $n_0(\vec{r})$ represents the ground state of the system. It should be noted that this separation permits expressing changes in physical properties of the system as a function of this small deformation density instead of dealing with the total electron density, resulting in an efficient scheme and a reduced computational cost.

3.3.2. The energy in second-principles density functional theory

Since the DFT energy obtained in Eq.(3.35) is a functional of the density, it is natural to think of implementing the aforementioned division of the density in such expression. By doing so, the only term which is non-linear, and therefore is not trivial to deal with, is the exchange and correlation functional $E_{xc}[n]$. However, provided that the deformation density $\delta n(\vec{r})$ is a small perturbation, we can expand $E_{xc}[n]$ as a function of $\delta n(\vec{r})$ about $n_0(\vec{r})$ as follows:

$$E_{xc}[n] = E_{xc}[n_0] + \int \left.\frac{\delta E_{xc}}{\delta n(\vec{r})}\right|_{n_0} \delta n(\vec{r}) d^3r + \frac{1}{2} \iint \left.\frac{\delta^2 E_{xc}}{\delta n(\vec{r}) \delta n(\vec{r}')}\right|_{n_0} \delta n(\vec{r}) \delta n(\vec{r}') d^3r d^3r' + \dots \,. \tag{3.38}$$

If we considered all terms in this expansion, the energy thus obtained would be the exact DFT energy. Nevertheless, since the deformation density $\delta n(\vec{r})$ is expected to be a small quantity, this expansion can be cut at second order without an excessive loss of accuracy. In fact, this approximation contains the full Hartree-Fock method, and so we can expect it to be accurate enough for our purposes. It is worth noting that, as it was mentioned at the beginning of this section, this method can be systematically improved by considering terms of higher order in Eq.(3.38).

The previous expansion of $E_{xc}[n]$ allows us to write the total energy as a sum of three terms, coming from the contributions of the deformation density at zeroth, first and second orders [24]:

$$E_{\text{DFT}} \approx E = E^{(0)} + E^{(1)} + E^{(2)} \,. \tag{3.39}$$

The zeroth order term, $E^{(0)}$, is the exact DFT energy for the reference density $n_0(\vec{r})$:

$$E^{(0)} = E_{\text{DFT}}(n_0(\vec{r}), \{\vec{R}\}) \,, \tag{3.40}$$

and it is typically modelled through an accurate force field that depends only on the atomic positions. The first order term, on the other hand, accounts for the one-electron excitations and it is given by the following expression:

$$E^{(1)} = \sum_{\boldsymbol{ab}} D_{\boldsymbol{ab}} \langle \chi_{\boldsymbol{a}} | \hat{h}_0 | \chi_{\boldsymbol{b}} \rangle \,, \tag{3.41}$$

where the particular shape that these matrix elements take in this work will be given in Subsection 3.5.2. These two terms, $E^{(0)}$ and $E^{(1)}$, play a key role in the present work. The second order term, however, represents the two-electron contribution and thus it is not relevant for our purposes.

3.4. Time-dependent second-principles density functional theory

In the previous section we have given an overview of the stationary second-principles density functional theory. However, a proper study of the transport properties of a solid requires a method capable to calculate both the current and the polarization as a function of time. Furthermore, as we are interested in the effect that temperature or external fields have on these properties, that method must be able to simulate non-equilibrium phenomena. For this reason, we shall consider here the extension into the time-domain of the SP-DFT, based on the method already described. In this section we shall give some essential notions of this approach, while a more detailed description can be found in Ref.[26].

The time-dependent second-principles density functional theory (TD-SPDFT) approach is based on the time propagation of the reduced density matrix using the equation of motion (EOM), and it can be expressed by the following equation, written also in the WFs basis [5]:

$$i\hbar\dot{\hat{n}}(t) = \left[\hat{n}(t), \hat{h}(t)\right] \iff \dot{d}_{\boldsymbol{ab}} = \frac{i}{\hbar}\sum_{\boldsymbol{c}}\left(\hat{h}'_{\boldsymbol{ac}}d_{\boldsymbol{cb}} - d_{\boldsymbol{ac}}\hat{h}'_{\boldsymbol{cb}}\right) , \tag{3.42}$$

where $\hat{h}'$ is the modified Hamiltonian involved in the propagation due to the fact that the Wannier functions are geometry-dependent and thus they vary over time.

As it has been mentioned, the objective in this section is to find the expression of the current $\vec{J}$ and the polarization $\vec{P}$ from a rigorously quantum-mechanical point of view, since these magnitudes determine the reaction of a material to external electric fields. Nevertheless, from a microscopical point of view, polarization in a solid is not a well-defined function and measurements can only capture its variations when a perturbation is applied, but not its absolute value. In Figure 3.1 below we show a cartoon which aims to illustrate this ambiguity for a periodic system under the action of an electric field.

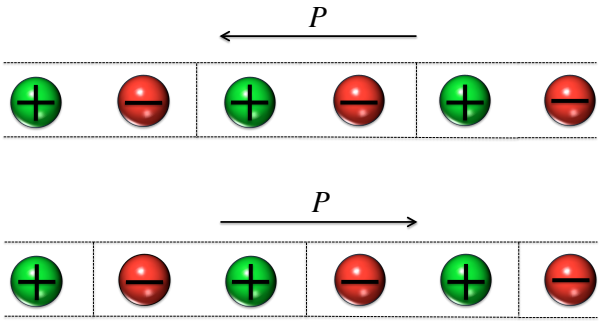

FIGURE 3.1. Schematic cartoon of a periodic system under the action of an external electric field. Since we can arbitrarily group the electric dipoles, there is not a unique definition for the polarization.

In fact, polarization in a solid was not clearly defined until King-Smith and Vanderbilt put forward their *modern theory of polarization* in the 90s [27, 28], and one key point of TD-SPDFT is that it is consistent with such theory [26].

Before giving the expressions of the current and the polarization in the TD-SPDFT approach, it should be noted that, although both magnitudes have a nuclear and an electron contribution, from now on we shall consider that the former is negligible compared with the latter, which is logical taking into account that the system under study in this work is a metal. Hence, we shall denote $\vec{J} \equiv \vec{J}_{elec}$ and $\vec{P} \equiv \vec{P}_{elec}$.

In the quantum mechanics framework, the current created by the electrons is defined as [29]:

$$\langle \vec{J}_{elec} \rangle = -\frac{e}{\Omega}\mathrm{Tr}\,\hat{n}\hat{\vec{v}} = \frac{e}{\Omega}\sum_{\boldsymbol{ac}}\left(\frac{1}{\hbar}d_{\boldsymbol{ac},i}\left[\hat{h},\vec{r}\right]_{\boldsymbol{ca}} - d_{\boldsymbol{ac},r}\frac{\partial\vec{r}_{\boldsymbol{ca}}}{\partial t}\right) , \tag{3.43}$$

where $\langle\cdot\rangle$ stands for the time average, Ω is the volume, and in the second equality we have expressed the velocity operator $\hat{\vec{v}}$ in the WFs basis.

On the other hand, the electron contribution to the polarization can be expressed as:

$$\vec{P}_{elec} = -\frac{e}{\Omega}\mathrm{Tr}\,\hat{n}\hat{\vec{r}} = -\frac{e}{\Omega}\sum_{ab} d_{ab}\vec{r}_{ba}\,, \tag{3.44}$$

where in the second equality we have written the position operator $\hat{\vec{r}}$ in the WFs basis. A more detailed deduction of these expressions can be found in Ref.[26].

Finally, it can be proved [26] that, with the preceding definitions, we have the following relation between the current and the polarization:

$$\langle\vec{J}\rangle = \frac{d\vec{P}}{dt}\,, \tag{3.45}$$

which coincides with the well-known classical expression [29].

3.5. Models

Thus far, in this chapter we have described the general formulation of the computational methods employed in this work, and now is the time to place the particular system that we aim to study within that framework. As it has been mentioned, one of the principal goals of this project is to properly understand the electrical conductivity in solids and its dependencies with the variations of the atomic geometry. For that purpose, we shall consider the simplest system which allows us to study these properties: a monoatomic linear chain with one electron per atom in a *s*-type orbital, embedded in a three-dimensional space. In this system, we shall let the atoms vibrate about the reference geometry, and we shall add the electron-lattice coupling between the electronic states and the lattice vibrations. Furthermore, the nearest-neighbour approximation will be also assumed, i.e. only interactions between nearest neighbours will be taken into account. A more detailed description of the individual models employed to describe each part of our system is given hereafter.

3.5.1. Harmonic force field

To model the lattice vibrations we have employed a force field that can be visualized, as we have seen during the degree, as though the atoms were rigid balls joined to each other by springs with a certain force constant [30]. Furthermore, here we shall consider the harmonic approximation, which consists on neglecting all terms above the second-order —the so-called anharmonic terms— in the expansion of the vibrational potential energy about the reference geometry [31]. Moreover, since the first-order term is zero because the reference geometry corresponds to a minimum of the APES, and the zeroth-order term is a constant that simply shifts the energy origin and, therefore, can be taken as zero without loss of generality, it turns out that the zeroth order terms of the SP-DFT energy is, in this case, the harmonic term of the vibrational energy. Therefore, $E^{(0)}$ depends solely on the difference of atomic positions, i.e. on the displacements of the nuclei with respect to their reference configuration. On the other hand, the hypothetical springs joining the atoms are characterized by a particular force constant, and given that the linear chain is embedded in a three-dimensional space, it is necessary to consider two different force constants: a longitudinal one, denoted as K_σ, associated to movements in the direction of the chain; and a transversal one, denoted as K_π, associated to shear modes. Given that longitudinal modes have higher energy —and hence higher frequency— than shear modes, we expect $K_\sigma > K_\pi$. Then, the force constant is not a scalar but a second-order tensor:

$$\overleftrightarrow{K} = \begin{bmatrix} K_\pi & 0 & 0 \\ 0 & K_\pi & 0 \\ 0 & 0 & K_\sigma \end{bmatrix}\,, \tag{3.46}$$

where we have associated the z-direction with the direction of the chain. Note that the two first diagonal terms are equal because the two transversal directions are equivalent. A schematic cartoon of this model is displayed in Figure 3.2.

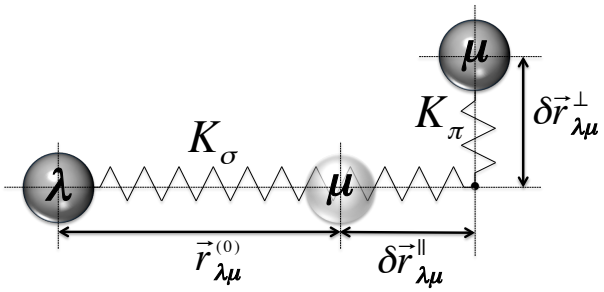

FIGURE 3.2. Cartoon which shows the principal components of the harmonic force field based on a spring model used to describe the lattice dynamics of the system, where we have distinguished between longitudinal and transversal movement of consecutive atoms $\boldsymbol{\lambda}$ and $\boldsymbol{\mu}$. Although this cartoon is two-dimensional, the actual system is embedded in a three-dimensional space where the two transversal directions are equivalent.

Therefore, the contribution to the total energy coming from the lattice vibrations, $E^{(0)}$, can be expressed as:

$$E^{(0)} = \frac{1}{2} \sum_{\boldsymbol{\lambda\mu}} \delta\vec{r}^{\,T}_{\boldsymbol{\lambda\mu}} \cdot \overleftrightarrow{K} \cdot \delta\vec{r}_{\boldsymbol{\lambda\mu}} \,, \tag{3.47}$$

where $\delta\vec{r}_{\boldsymbol{\lambda\mu}} = \vec{r}_{\boldsymbol{\lambda\mu}} - \vec{r}^{\,(0)}_{\boldsymbol{\lambda\mu}}$ is a vector denoting the relative displacement of consecutive atoms $\boldsymbol{\lambda}$ and $\boldsymbol{\mu}$.

3.5.2. Tight-binding and electron-lattice interaction

The electronic part of the system, namely the electronic states and the energy bands, corresponding in second-principles to the term $E^{(1)}$ shown in Eq.(3.41), is modelled through a tight-binding mechanism, an approach that has also been seen during the degree, and which can be considered as the equivalent for solids of the linear combination of atomic orbitals (LCAO) for molecules [17]. In this case, the basis of atomic orbitals is formed by the already introduced Wannier functions $\{|\chi_{\boldsymbol{a}}\rangle\}$, which, given their localization, are adequate to reproduce the s-type orbitals of the chain.

In every tight-binding scheme there are two principal magnitudes that characterize the interactions between the atomic orbitals, namely the overlap between the orbitals and the hopping or resonance integral [32]. In this case, $|\chi_{\boldsymbol{a}}\rangle$ and $|\chi_{\boldsymbol{b}}\rangle$ are WFs and the overlap is given by:

$$S_{\boldsymbol{ab}} = \langle\chi_{\boldsymbol{a}}|\chi_{\boldsymbol{b}}\rangle = \delta_{\boldsymbol{ab}} \,, \tag{3.48}$$

where $\delta_{\boldsymbol{ab}}$ is the Kronecker delta, since the WFs are orthogonal. The fact that this overlap integrals vanish evinces one of the great virtues of the aforementioned basis, since the calculation of those integrals is usually computationally demanding when dealing with non-orthogonal basis functions.

The second fundamental magnitude of the tight-binding model is the hopping or resonance integral between two orbitals $|\chi_{\boldsymbol{a}}\rangle$ and $|\chi_{\boldsymbol{b}}\rangle$:

$$\gamma_{\boldsymbol{ab}} = \langle\chi_{\boldsymbol{a}}|\,\hat{h}_0\,|\chi_{\boldsymbol{b}}\rangle \,, \tag{3.49}$$

which is the matrix element involved in the expression of $E^{(1)}$ shown in Eq.(3.41). Since the computation of this matrix element involves the one-electron Hamiltonian, which contains the electrostatic interactions, $\gamma_{\boldsymbol{ab}}$ should have, in principle, both long-range and short-range

contributions. In fact, this would permit accounting for interactions with distant neighbours, but, since in this work we assume the nearest-neighbour approximation, we shall only consider the short-range electrostatic contribution to γ_{ab}. Hence, under such approximation, we can write:

$$\gamma_{ab} = \begin{cases} \gamma & \text{if } \boldsymbol{a}, \boldsymbol{b} \text{ are nearest neighbours,} \\ 0 & \text{otherwise.} \end{cases} \tag{3.50}$$

When $\boldsymbol{a} = \boldsymbol{b}$, instead of hopping we call it *on site* energy:

$$\alpha \equiv \alpha_{\boldsymbol{a}} = \gamma_{\boldsymbol{aa}} \,. \tag{3.51}$$

Although in Eq.(3.50) we have introduced γ_{ab} as a constant, it actually presents a dependence on the atomic geometry, or rather with the variation thereof with respect to the RAG. In the SP-DFT approach, this dependence is expressed through the electron-lattice coupling, which under the nearest-neighbour approximation is given by:

$$\gamma = \gamma_0 - \vec{f}_{\boldsymbol{\lambda\mu}} \delta\vec{r}_{\boldsymbol{\lambda\mu}} \,, \tag{3.52}$$

for any two consecutive atoms $\boldsymbol{\lambda}$ and $\boldsymbol{\mu}$. In this expression $\vec{f}_{\boldsymbol{\lambda\mu}}$ is a first-rank tensor whose module is $f_{\boldsymbol{\lambda\mu}}$ and whose direction is the one of the chain, and which will be called from now on the electron-lattice parameter. In fact, Eq.(3.52) comes from the expansion of γ about the RAG, which, provided that the atomic displacements are small compared with the interatomic spacing, can be cut at first-order. Hence, the electron-lattice parameter is given by:

$$\vec{f}_{\boldsymbol{\lambda\mu}} = -\vec{\nabla}\gamma\Big|_{\delta\vec{r}_{\boldsymbol{\lambda\mu}}=0} \,. \tag{3.53}$$

As reasoned for γ_{ab}, since we shall only consider interactions with nearest neighbours, the electron-lattice parameter can be rewritten as:

$$\vec{f}_{\boldsymbol{\lambda\mu}} = \begin{cases} \vec{f} & \text{if } \boldsymbol{\lambda}, \boldsymbol{\mu} \text{ are nearest neighbours,} \\ 0 & \text{otherwise.} \end{cases} \tag{3.54}$$

An example that can be quite illustrative about the electron-lattice interaction is the Peierls distortion, a problem that will be briefly analysed in the following chapter.

Thus, as a result of what has been stated up to now, the one-electron contribution to the total energy will be given by:

$$E^{(1)} = \sum_{\boldsymbol{ab}} D_{\boldsymbol{ab}}\gamma_{\boldsymbol{ab}} = \sum_{\boldsymbol{a}} \alpha D_{\boldsymbol{aa}} + \gamma \left(D_{\boldsymbol{a,a+1}} + D_{\boldsymbol{a,a-1}} \right) \,. \tag{3.55}$$

We have already finished the description of our system and all the pieces of which it is composed. Figure 3.3 shows a cartoon with its principal elements and interactions, which can help to visualize it as a whole.

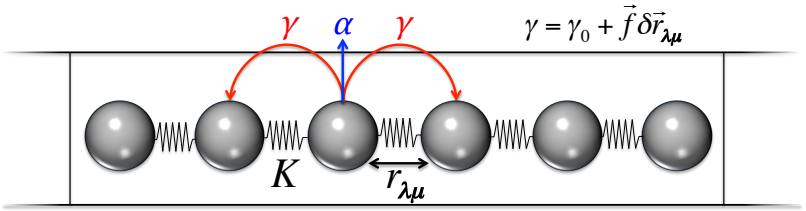

FIGURE 3.3. Schematic cartoon of the linear chain studied in this work where its three principal components can be observed, namely the harmonic force field (springs), the tight-binding interactions and the electron-lattice coupling.

3.6. The SCALE-UP package and model parameters

Before finishing this chapter it is necessary to make a few comments on the software employed in this work to perform the second-principles simulations. In our study we have used the SCALE-UP package [33], which implements the second-principles methods described in preceding sections. The completely rigorous manner to proceed would consist on performing the first-principles simulations and then using the results for one-electron Hamiltonians as input for the second-principles simulations. However, this exceeded the scope of this work, and since our purpose here is to acquire a qualitative comprehension of transport properties of solids, instead of studying a real material we have made here a systematic study of the effect of the system parameters introducing them by hand. Nevertheless, the study of real materials through first and second-principles simulations constitutes a possible extension of this dissertation.

CHAPTER 4

Results and Discussion

Introduction. Once the computational and conceptual background of this work has been laid down, it is time to present and discuss the results obtained in this work. We shall start by showing the influence of the hopping parameter and the size of the supercell on the energy bands, and the dispersion curves associated to the lattice vibrations of the chain. Afterwards, we shall briefly study the interesting phenomenon of Peierls distortion as a first example to illustrate the electron-lattice interaction. Then, we shall continue by presenting the principal result of this work: the evolution from Bloch oscillations at $T = 0\,\mathrm{K}$ when an external, static electric field is applied, into ohmic transport when the temperature is increased. Likewise, a simple model devised to explain Bloch oscillations will be described. Finally, we shall discuss the various trends with the applied electric field, the band width, the phonon frequency and the electron-lattice coupling by presenting the results obtained from systematic second-principles simulations. It should be remarked that our aim here was not to develop quantitatively precise calculations but to conduct a qualitative study of different properties related to transport in solids as an attempt to provide with a better understanding of that field.

Contents

4.1. Energy bands

As it was mentioned in the preceding chapter, in this work the electronic structure is modelled, essentially, through a tight-binding mechanism. Hence, in this section we aim to show the energy bands corresponding to the system under study in this work, described in Section 3.5, with a view to illustrate this part of the model. Since at this moment we are only concerned with the electronic bands, in this section we shall not consider the electron-lattice coupling, i.e. even though the atoms are allowed to vibrate, the effect that this atomic displacements have on the energy bands will be neglected. In practice, this is equivalent to consider that the electron-lattice constant, described in Eq.(3.54), is equal to zero. In order to better understand the following results, we shall first illustrate the concept of band folding. In Figure 4.1 we show the results obtained from the simulations for the energy bands corresponding to the linear chain in the absence of electron-lattice interaction. The number of atoms of the supercell was increased from 1 to 15.

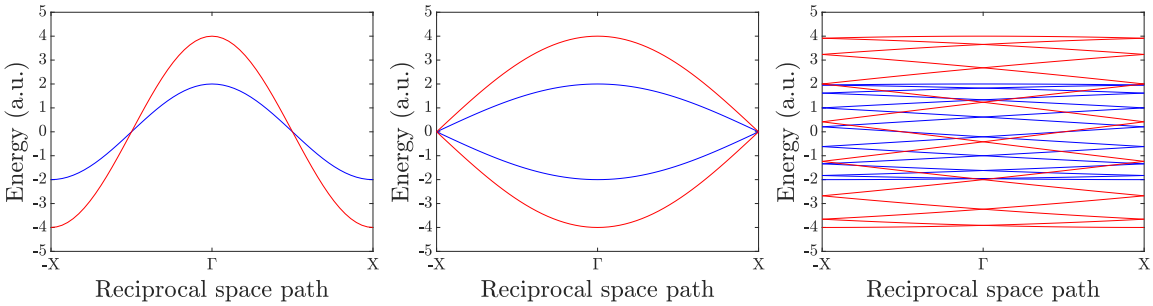

(a) 1 atom per cell (b) 2 atoms per cell (c) 15 atoms per cell

FIGURE 4.1. Tight-binding energy bands of a one-dimensional chain for two different values of the hopping parameter, $\gamma = 1\,\text{eV}$ (blue) and $\gamma = 2\,\text{eV}$ (red), and three different sizes of the supercell: (a) 1 atom per cell, (b) 2 atoms per cell and (c) 15 atoms per cell. The band folding phenomenon is clearly observed.

Although at first glance it might appear that the results obtained are quite different, the three graphs show indeed the same physical system. What actually happens is that the number of bands coincides with the degrees of freedom of the wave function, i.e. the number of different atomic orbitals involved. Thus, when considering two identical atoms per cell, we are not dealing with a diatomic chain of lattice parameter $a_0 = 2a$, but with the same monoatomic chain that we had when considering one atom per cell. Given that the X point (the edge of the first Brillouin zone) in the reciprocal space is $\frac{2\pi}{a_0}$, when considering double supercells the reciprocal space folds in half, etc. Therefore, if we unfolded the lower band just after the upper band we would obtain the same figure as in Figure 4.1(a). Of course, an analogous reasoning applies for the case of fifteen atoms per cell.

Having made this clear, it is necessary to make a few brief comments on the band occupation. Since for each band there are N_c $\vec{k}$ states, where N_c is the number of primitive cells, and each one of these states corresponds to two spin possibilities, it follows that each band can accommodate $2N_c$ electrons. Hence, as our system is composed by monolectronic atoms, it turns out that only the lower half of the first band will be filled, and thus the Fermi level will lie in the middle of such band. Consequently, our system is a metal, as it has been already mentioned.

4.2. Lattice vibrations and dispersion curves

Continuing with this brief presentation of the results corresponding to the individual components of our model, in this section we aim to illustrate the lattice dynamics of the chain, modelled, as aforementioned, through a harmonic force field similar to a spring model in which the forces between the atoms can be described as though they were joined by springs with a force constant that is indeed a second-order tensor, as written in Eq.(3.46), which contains both a longitudinal and a transversal force constant. As here we shall focus on the ionic part of the system, the electronic part will be forgotten until the next section.

If we consider one atom per cell, i.e. $N_c = 1$, and we allow the atoms to vibrate in the three directions of the space, i.e. there are three degrees of freedom per atom, the expected dispersion curves obtained when studying the relationship between the phonon frequency and the wave vector $\vec{k}$ in the direction of the chain will consist of three acoustic branches, one of which corresponds to the longitudinal mode while the other two branches account for the two transversal modes. The results obtained through the simulations for the phonon dispersion curves of our one-dimensional chain are shown in Figure 4.2.

As it was mentioned in the previous chapter, we have considered K_σ to be greater than K_π in order to be coherent with the fact that the sound velocity, i.e the slope of the dispersion

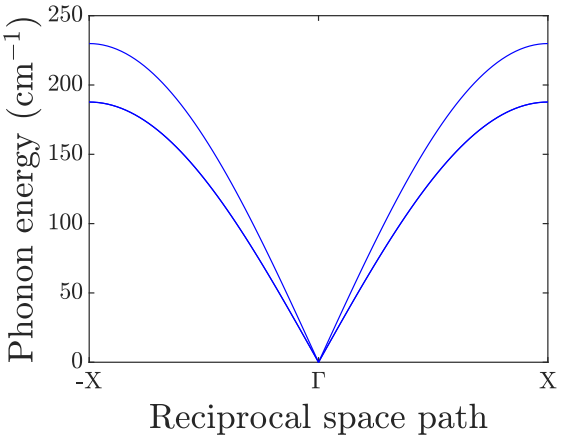

FIGURE 4.2. Phonon dispersion curves of a one-dimensional chain with one atom per cell, embedded in a three-dimensional space. Since there are two spatial directions which are equivalent, both transversal modes are degenerated. The characteristic sinusoidal form of the dispersion curves for the acoustic modes can be clearly appreciated.

curve when $\vec{k}$ tends to zero, is always greater in longitudinal modes than in the transversal ones, since the former involve shrinkage and stretch of the bonds while the latter are related to the bending of these bonds, which is energetically less demanding, and then we shall necessarily have $K_\pi < K_\sigma$ and therefore $\omega_\pi < \omega_\sigma$.

Although in previous paragraphs we have mentioned that three acoustic branches would be obtained when representing the dispersion curves of the chain, in Figure 4.2 it appears to be only two of them. Nevertheless, the three branches are indeed present, and what actually happens here is that the two transversal ones are degenerated owing to the fact that the two directions which are perpendicular to the linear chain are spatially equivalent. Thus, in Figure 4.2 the upper curve corresponds to the longitudinal mode while the lower curve includes both transversal modes.

It should be remarked that the same reasoning set out in the preceding section about the size of the supercell applies equally here, and hence we have only presented the results for the case of one atom per cell.

4.3. Peierls distortion: electron-lattice interaction

Perhaps one of the simplest phenomena in which the electron-lattice coupling plays a fundamental role is the Peierls distortion in a linear chain, also known as Peierls transition or dimerization. Therefore, because of its simplicity and illustrative power, it was one of the first systems studied in this work using second-principles simulations in our path towards the understanding of the electron-lattice interaction. Although Peierls originally described distortion phenomena for different systems [34], here we shall consider a monoatomic linear chain, the same system studied in the rest of this dissertation.

Hence, imagine a linear chain with lattice parameter a, and all their atoms equally spaced, as it is shown in the upper picture of Figure 4.3(a). In these conditions, the system is perfectly periodical and the lattice vectors are multiples of a. The corresponding band diagram for this system is the one displayed in Figure 4.1, and it has been already reasoned why the three diagrams of that figure are equivalent in this case. Thus, let us consider here the linear chain formed by supercells containing two atoms. Then, the first Brillouin zone will be $-\frac{\pi}{2a} < k < \frac{\pi}{2a}$. As it can be observed in Figure 4.1, when the system is undistorted there is no gap between the upper and the lower band. However, if we slightly distort the chain by displacing each

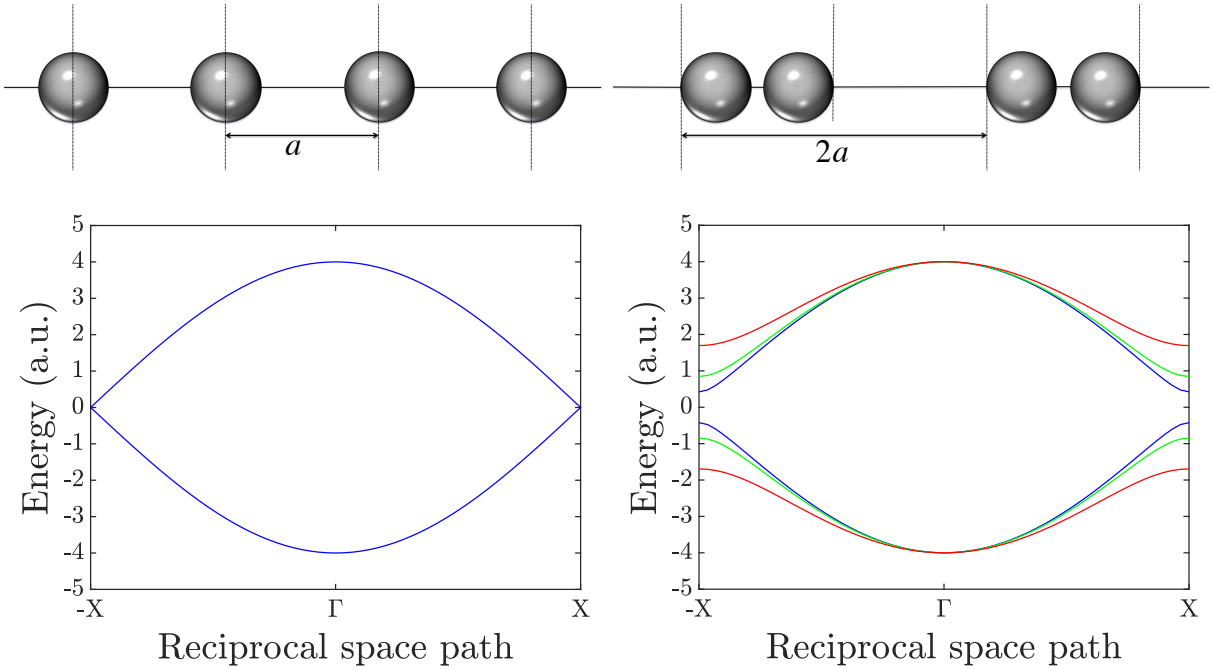

(a) Undistorted (b) Distorted

FIGURE 4.3. Peierls distortion in a one-dimensional chain with two atoms per cell due to the electron-lattice interaction. In (a) the band diagram corresponding to the undistorted chain presents no gap between the upper and the lower bands, but when the electron-lattice coupling is taken into account, the translational symmetry breaking induces a gap between the bands, as it can be observed in (b), where the band diagram has been plotted for three different values of the electron lattice constant: $f = 1\,\mathrm{eV\,Å^{-1}}$ (blue), $f = 2\,\mathrm{eV\,Å^{-1}}$ (green) and $f = 4\,\mathrm{eV\,Å^{-1}}$ (red).

atom a little, this displacement repeated every two atoms, the translational symmetry that we had before is immediately broken and the lattice parameter becomes $2a$, as it has been sketched in Figure 4.3(b). Of course, if we do not consider the coupling between the lattice vibrations and the electronic states, the band diagram will not be affected by the distortion, but if we introduce the electron-lattice interaction described in Subsection 3.5.2, the translational symmetry breaking induces a gap between the lower and the upper bands which depends on the value of the electron-lattice constant, as it is illustrated in the band diagram of Figure 4.3(b).

From this phenomenon it follows that if the edge of the Fermi distribution coincides with the centre of the gap displayed in Figure 4.3(b), the states which are displaced downwards in energy will be occupied while the states which are raised will be empty, resulting in a net reduction of the energy. As a consequence, it turns out that for a one-dimensional metal with a half filled band the regular chain structure will not, in principle, be stable, and thus in these conditions the atoms tend to close up in pairs forming a molecular lattice [34].

4.4. From Bloch oscillations to ohmic transport using SP-DFT

After describing the results concerning the individual elements of the model, in this section we aim to present the principal results of this work. First, we shall show the results corresponding to the case $T = 0\,\mathrm{K}$, for which the already mentioned Bloch oscillations will be observed, and we shall try to justify their behaviour when an electric field is applied using a two-level model; after that, we shall check how these oscillations are distorted when the temperature is increased, until reaching the ohmic transport for the case $T = 300\,\mathrm{K}$. For this temperature, as it was mentioned in the introduction of this chapter, we shall also present the results corresponding

to the systematic study of the dependence of the current and the polarization on the different parameters of the system. From now on, the results displayed will correspond to a supercell size of 15 atoms.

4.4.1. Bloch oscillations in the absolute zero

The first step in our path towards the understanding of electronic transport and conductivity was the second-principles simulation of our linear chain for a fixed temperature $T = 0\,\mathrm{K}$. For this temperature, the atoms of the chain can be considered completely frozen (the zero-point vibrations are neglected) and, therefore, we have a perfectly periodic crystal. Thus, according to what it was mentioned in the introduction of this work, there is not any resistivity mechanism and, consequently, if we applied an electric field to this system, we would expect to observe an oscillatory behaviour for the current and the polarization. This is indeed what happens, as it can be observed in Figure 4.4. In this simulations, the applied electric fields are unrealistically large and no measurements would exist for these values; however, since the period of Bloch oscillations is inversely proportional to the amplitude of the electric field, we have chosen such large values in order to observe Bloch oscillations in a reasonable computation time. It should also be noted that many of the simplifying assumptions of the semiclassical model are not present here.

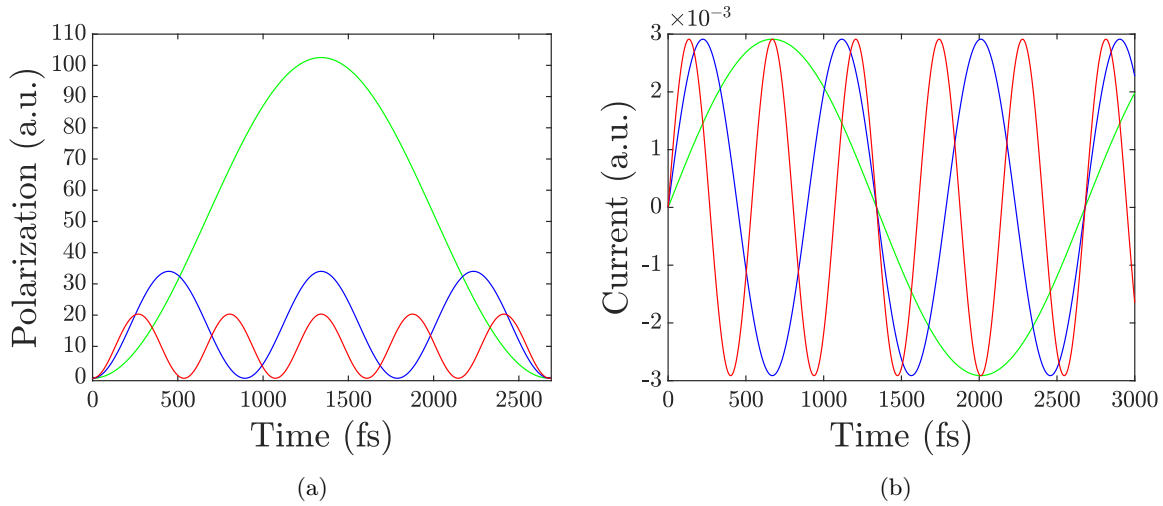

(a) (b)

FIGURE 4.4. Current and polarization of the linear chain under the action of a static electric field for the case $T = 0\,\mathrm{K}$, where the oscillatory behaviour of these magnitudes can be clearly observed. In order to show the dependence of the frequency and the amplitude of the Bloch oscillations on the applied electric field, we have plotted here the results for $\vec{E}_{int} = 5.14 \times 10^6\,\mathrm{V\,m^{-1}}$ (green), $\vec{E}_{int} = 1.54 \times 10^7\,\mathrm{V\,m^{-1}}$ (blue) and $\vec{E}_{int} = 2.57 \times 10^7\,\mathrm{V\,m^{-1}}$ (red). As it can be appreciated, the higher the electric field, the higher the frequency of the oscillations and the lower the amplitude thereof.

As it can be appreciated in Figure 4.4(a) above, the magnitude of the applied electric field has two effects. On the one hand, we observe the well-known relation between such magnitude and the frequency of the oscillations, expressed in Eq.(2.15). On the other hand, it can be noted how, in the case of the polarization, the intensity of the oscillations decreases as the magnitude of the applied electric field is increased, a less known phenomenon which, in general, remains unexplained in most of the textbooks. Thus, in order to provide some insight into this problem, a simple model which accounts for the aforementioned phenomena has been devised.

4.4.1.1. A two-level model to explain Bloch oscillations

In order to provide with a theoretical justification for the phenomena observed in Figure 4.4, let us consider a system with lattice parameter a formed by two energy levels, represented by

two localized orbitals (e.g. Wannier functions), $|\chi_1\rangle$ and $|\chi_2\rangle$, which constitute a discrete basis $\{|\chi_i\rangle\}$. Hence, we can express the wave function of any state $|\psi\rangle$ of the system at a time $t > 0$ in this basis as:

$$|\psi(t)\rangle = \sum_{i=1}^{2} c_i(t)\,|\chi_i\rangle \ , \tag{4.1}$$

where the coefficients c_i are given by:

$$c_i(t) = \langle\chi_i|\psi(t)\rangle \ . \tag{4.2}$$

In fact, this is a very simple case of a Wannier-Stark ladder with only two orbitals, and it is of great interest, since it can be solved analytically. A schematic cartoon of the system is shown in Figure 4.5.

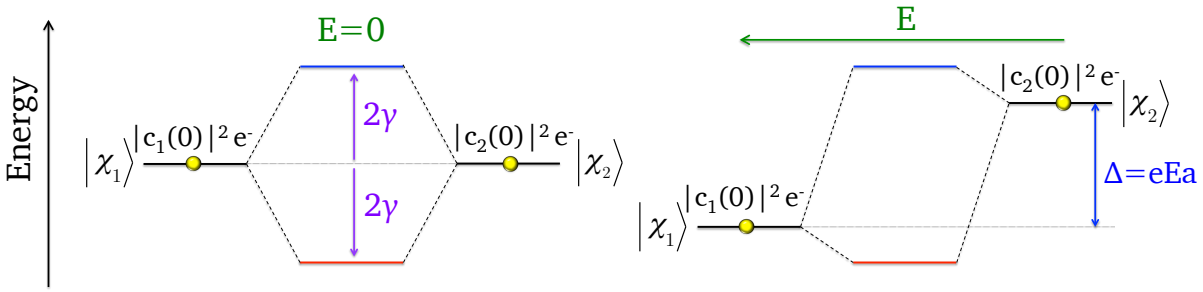

FIGURE 4.5. Schematic cartoon which represents a system consisting on two energy levels, where the energy difference depends on the applied electric field $\vec{E}$ and the lattice parameter a.

Initially, the orbitals $\{|\chi_i\rangle\}$ have the same energy and the potential energy of the system is just the crystalline potential $V(\vec{r})$, but, when an external electric field $\vec{E}$ is applied, such degeneracy is broken because the potential energy becomes $V(\vec{r}) - e\vec{E}\vec{r}$ and thus these levels become separated by an energy difference $\Delta = eEa$. Moreover, the interaction energy γ between the orbitals should also be taken into account. Therefore, the Hamiltonian matrix can be expressed in the basis $\{|\chi_i\rangle\}$ as:

$$\hat{h} = \begin{pmatrix} -\Delta/2 & \gamma \\ \gamma & \Delta/2 \end{pmatrix} . \tag{4.3}$$

Our aim here is to obtain the temporal evolution of the occupation matrix d_{ab}, so we need to know the expression of $c_i(t)$. To this end, we shall solve the Schrödinger equation:

$$i\hbar\,|\dot{\psi}(t)\rangle = \hat{h}\,|\psi(t)\rangle \ , \tag{4.4}$$

where $|\dot{\psi}(t)\rangle$ denotes the time derivative of $|\psi(t)\rangle$. For the sake of simplicity, the Hamiltonian matrix should be diagonalized. The eigenvalues of (4.3) are:

$$\lambda_1 = \sqrt{(\Delta/2)^2 + \gamma^2}\,, \quad \lambda_2 = -\sqrt{(\Delta/2)^2 + \gamma^2}\,, \tag{4.5}$$

and the correspondent eigenstates of the Hamiltonian are:

$$|v_1\rangle = \begin{pmatrix} \dfrac{-\Delta/2 - \sqrt{(\Delta/2)^2 + \gamma^2}}{\gamma} \\ 1 \end{pmatrix} , \quad |v_2\rangle = \begin{pmatrix} \dfrac{-\Delta/2 + \sqrt{(\Delta/2)^2 + \gamma^2}}{\gamma} \\ 1 \end{pmatrix} . \tag{4.6}$$

The matrix (4.3) written in the basis $\{|v_i\rangle\}$ is a diagonal matrix whose diagonal elements are the correspondent eigenvalues. Then, the equation (4.4) can be written as follows:

$$i\hbar \begin{pmatrix} \dot{c}'_1 \\ \dot{c}'_2 \end{pmatrix} = \begin{pmatrix} \sqrt{(\Delta/2)^2 + \gamma^2} & 0 \\ 0 & -\sqrt{(\Delta/2)^2 + \gamma^2} \end{pmatrix} \begin{pmatrix} c'_1 \\ c'_2 \end{pmatrix} , \tag{4.7}$$

where we use the " $'$ " character to express that we are working on the new basis $\{|v_i\rangle\}$. Thus, we have to solve two first-order differential equations, whose solutions are well known and are given by:

$$c_1'(t) = c_1'(0)e^{\frac{-it\sqrt{(\Delta/2)^2+\gamma^2}}{\hbar}}, \tag{4.8}$$

$$c_2'(t) = c_2'(0)e^{\frac{it\sqrt{(\Delta/2)^2+\gamma^2}}{\hbar}}. \tag{4.9}$$

Nevertheless, the expression of the coefficients $c_i'(0)$ in the basis $\{|v_i\rangle\}$ remains unknown. To find it, a change of basis should be done. After doing some matrix algebra, we finally obtain:

$$c_1(t) = \left[\frac{-i\Delta/2}{\sqrt{(\Delta/2)^2+\gamma^2}}\sin(\omega t) + \cos(\omega t)\right] c_1(0) + \left[\frac{i\gamma}{\sqrt{(\Delta/2)^2+\gamma^2}}\sin(\omega t)\right] c_2(0)\,, \tag{4.10}$$

$$c_2(t) = \left[\frac{i\gamma}{\sqrt{(\Delta/2)^2+\gamma^2}}\sin(\omega t)\right] c_1(0) + \left[\frac{i\Delta/2}{\sqrt{(\Delta/2)^2+\gamma^2}}\sin(\omega t) + \cos(\omega t)\right] c_2(0)\,. \tag{4.11}$$

where $\omega = \sqrt{(\Delta/2)^2+\gamma^2}/\hbar$. Once we have found the expression of these coefficients, we can discuss the behaviour of the system depending on the initial occupation $|c_i(0)|^2$ of each level. If we consider the case in which one orbital is initially occupied and the other is initially empty, there are two possibilities for the initial coefficients of the wave function: either $c_1(0) = 1$ and $c_2(0) = 0$, in which case the initial wave function is $|\psi(0)\rangle = |\chi_1\rangle$; or $c_1(0) = 0$ and $c_2(0) = 1$, in which case the initial wave function is $|\psi(0)\rangle = |\chi_2\rangle$. In both cases, the initial wave function will be an atomic orbital. In Figure 4.6 we show the temporal evolution of the occupation in both cases for two different values of the applied electric field.

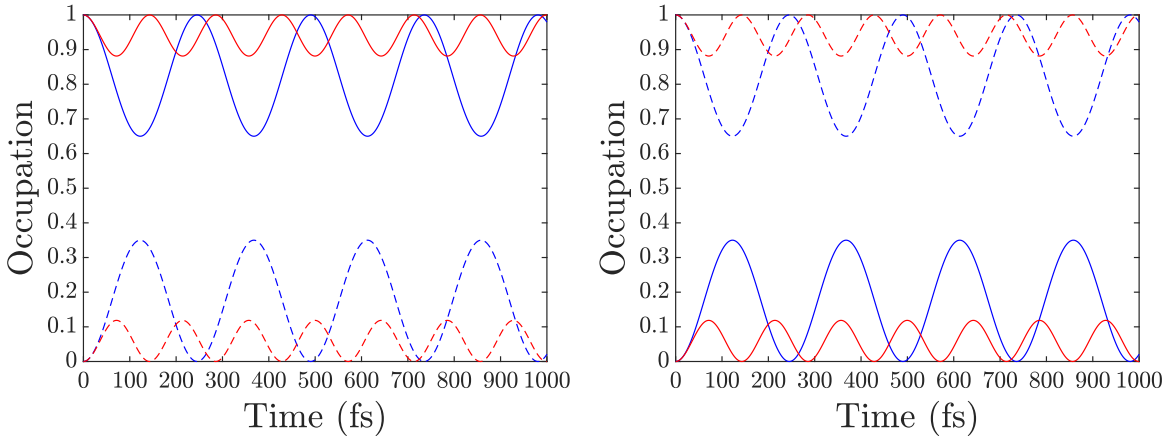

(a) $c_1(0) = 1$, $c_2(0) = 0$ (b) $c_1(0) = 0$, $c_2(0) = 1$

FIGURE 4.6. Temporal evolution of the occupation of the two levels when one of them is initially filled and the other is initially empty, for two different amplitudes of the applied electric field: $\vec{E}$ (blue) and $2\vec{E}$ (red). The continuous line corresponds to the orbital $|\chi_1\rangle$ and the dotted line, to the orbital $|\chi_2\rangle$. It should be noted that the temporal evolution of the occupation presents an oscillatory behaviour, and that the frequency and the amplitude of the oscillations depend on the amplitude of the applied electric field.

First of all, it should be noted that, even though the system at $t = 0$ is in a defined state $|\chi_i\rangle$, there is a certain probability, which can be obtained from the so-called Rabi's formula, of finding

it in the state $|\chi_j\rangle$ $(i \neq j)$ at time t. A detailed deduction of that formula and a more thorough discussion of different phenomena related to two-level systems can be found in Ref.[5].

It can be appreciated in Figure 4.6 that the occupation presents an oscillatory behaviour, which would give rise to an oscillatory electric current. In fact, we observe a dependence of the frequency and the amplitude of the oscillations on the electric field which is similar to that of the Bloch oscillations shown in Figure 4.4. The fact that the amplitude of the oscillations decreases as the electric field is increased is quite intuitive, since increasing the amplitude of the applied electric field implies a greater energy difference between the orbitals, which causes that, even though the changes in the occupation are faster, the electrons are much more localized in their respective orbitals.

If we focus our attention on Figure 4.6(b), in which the electron is initially in the higher energy level, one might intuitively think that the electron should spend more time in the lower energy level in order to minimize the potential energy of the system. However, what we observe is that the electron spends most of the time in the upper level. To justifiy this behaviour, we shall take advantage of the fact that this particular case has a classical analogous. Hence, imagine that the electron is confined within a double-well potential like the one sketched in Figure 4.7.

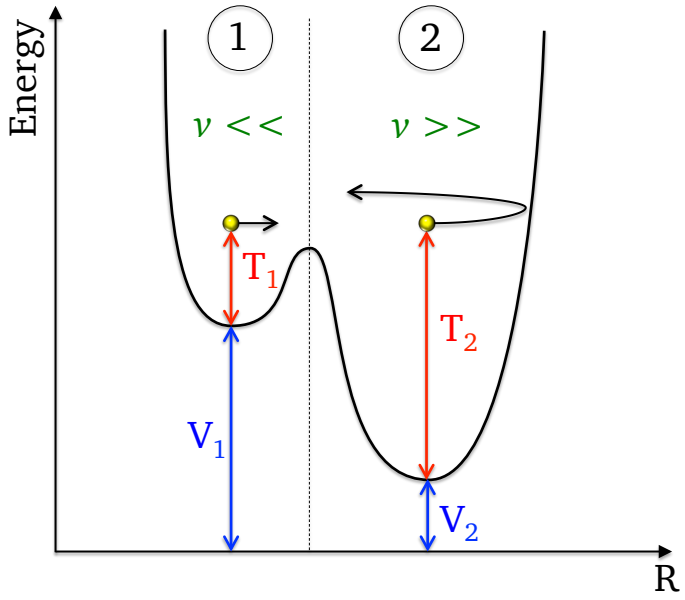

FIGURE 4.7. Schematic cartoon of a double-well potential. We have denoted the kinetic and potential energy of the electron in the region i as T_i and V_i respectively. Since the kinetic energy is much greater in the second region that in the first one, the electron will move much faster in the second one.

As it was mentioned in the previous paragraph, at first glance one might think that the electron should tend to be the region 2 in order to minimize the potential energy. However, the kinetic energy in that region is very high and, consequently, the electron will move very fast, so that it will take a short time to return to the region 1, where the kinetic energy is lower and the movement of the electron is, therefore, slower. As a consequence, the electron will spend more time in the region 1, as we observe in Figure 4.6(b).

On the other hand, if the electron is initially in the lower energy level, it will not have enough energy to reach the higher level and, therefore, will spend most of the time in the lower level, as shown in Figure 4.6(a).

4.4.2. Distortion of Bloch oscillations with temperature

Once we have studied what happens when we consider the absolute zero case and we have seen how Bloch oscillations emerge in that case, the next step is to study what occurs when the

temperature is gradually increased until reaching the room one. It should be remarked once again that being able to deal with finite temperatures constitutes one of the greatest advantages of second-principles simulations with respect to first-principles.

In accordance with what was set out in the second chapter of this work, when we increase the temperature from 0 K up to a finite one, the vibrational energy of the system is increased and the atoms begin to vibrate around their reference positions with amplitudes that are proportional to the temperature, as it was schematically shown in Figure 2.1. As it was mentioned, these vibrations break the perfect periodicity of the solid, and the differences with the ideal, perfect lattice increase quantitatively with temperature. Thus, this collapse of the periodicity will cause a distortion on the Bloch oscillations which will depend on the temperature of the system. In order to illustrate the effect of atomic vibrations in an intermediate situation between the absolute zero and the room temperature, we show in Figure 4.8 the results obtained for the current and the polarization of the linear chain at a temperature $T = 100\,\mathrm{K}$.

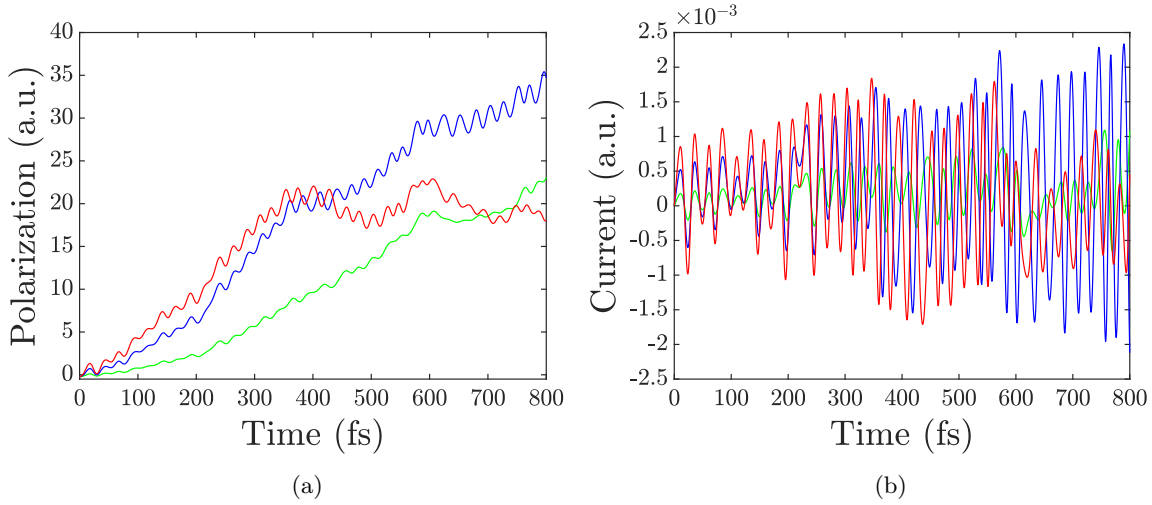

(a) (b)

FIGURE 4.8. Results obtained for the current and the polarization on a one-dimensional linear chain for $T = 100\,\mathrm{K}$ and three different values of the applied electric field: $\vec{E}_{int} = 5.14 \times 10^6\,\mathrm{V\,m^{-1}}$ (green), $\vec{E}_{int} = 1.54 \times 10^7\,\mathrm{V\,m^{-1}}$ (blue) and $\vec{E}_{int} = 2.57 \times 10^7\,\mathrm{V\,m^{-1}}$ (red). It can be appreciated the distortion of the Bloch oscillations with respect to the case $T = 0\,\mathrm{K}$ shown in Figure 4.4.

As it can be appreciated in the previous figure, the oscillations, which at $T = 0\,\mathrm{K}$ presented a perfect sinusoidal form, are now notably distorted due to the loss of periodicity of the system. As we shall see, these distortions will be more and more significant as the temperature is increased, until reaching a value for which the effect of the scattering of the electrons by the phonons is so strong that the former will be transported only in one direction, resulting in the ohmic transport that we are accustomed to observing under normal conditions.

4.4.3. Ohmic transport at room temperature. A systematic study

In the following subsections we show the results obtained through the second-principles simulations carried out at a temperature $T = 300\,\mathrm{K}$. A systematic study of the dependence of the system on its different parameters has been conducted in order to properly understand its influence on the transport properties of our system. The size of the supercell for all of that calculus has been 15 atoms. It should be noted that, in the cases in which fitting the curve of the polarization to a line is justified, only times above 2000 fs have been considered, since from thereon the system is already thermalized in all cases.

4.4.3.1. Dependence on the electric field

As a first step in the systematic study of the parameter space of our system, let us see how the current and the polarization vary when we change the amplitude of the applied electric field. Given that at a temperature $T = 300\,\mathrm{K}$ the system should present an ohmic behaviour, we can expect the current to increase proportionally to the increment of the applied electric field, being the proportionality constant the conductivity σ of the system, as expressed in Eq.(1.2). Figure 4.9 shows the results obtained for different amplitudes of the electric field.

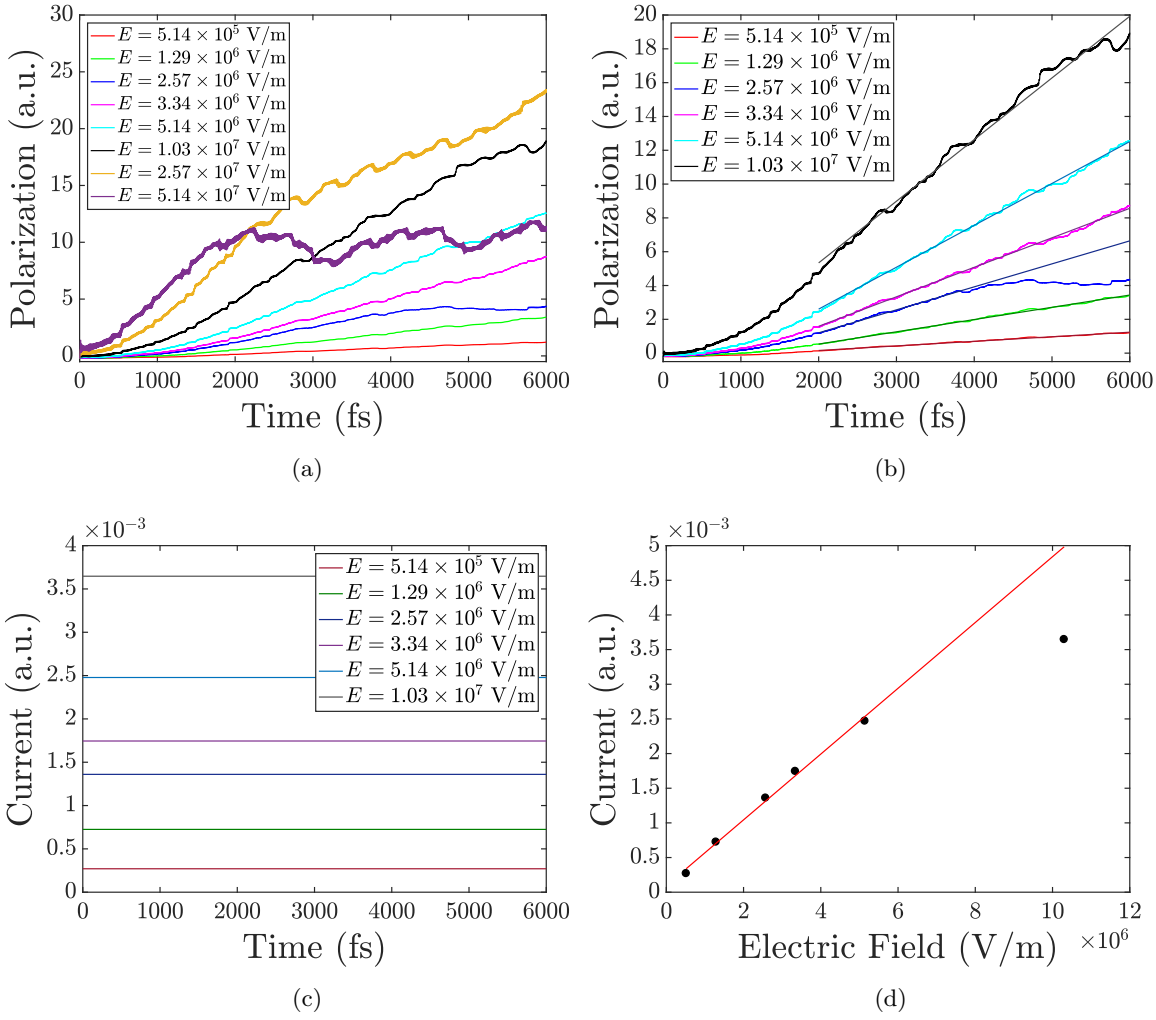

Figure 4.9. Dependence of the current and the polarization of the linear chain on the applied electric field. In figure (a) it can be observed that, for very large electric fields, Bloch oscillations dominate.

In the figure above we can observe, at first glance, mainly two effects. On the one hand, it can be noted that when the electric field reaches sufficiently large values, the polarization is not a line anymore, but it presents oscillations, in a similar way to the Bloch oscillations observed in the case $T = 0\,\mathrm{K}$. A possible explanation to this phenomenon is that, for such large values of the applied electric field, the period of the Bloch oscillations is shorter than the relaxation time of the scattering of the electrons by the phonons, which allows us to observe the oscillations once the system is thermalized. On the other hand, it can be observed that the current increases when the electric field does. In order to check if this dependence of the electric current on the amplitude of the applied electric field presents an ohmic behaviour, in Figure 4.9(d) we have shown the values of the current as a function of the electric field. As it can be appreciated, for

not very large values of the electric field the system presents an ohmic behaviour and Eq.(1.2) is verified. However, if we continue increasing the amplitude of the electric field, there comes a point where such law is no longer valid, since for such large fields Bloch oscillations begin to gain importance.

4.4.3.2. Dependence on the band width

Another parameter of great relevance in this systematic study of the transport properties of our linear chain is the hopping parameter γ, introduced in section 3.5. Its importance lies in the fact that the conductivity is proportional to the group velocity of the energy bands [29], that is, the slope of the tangent line at each point. As it can be appreciated in Figure 4.1, this slope increases as the band width does, and this band width is in turn proportional to the hopping parameter γ —the band width is 4γ—. Therefore, it follows that the conductivity of the system has to be proportional to the hopping parameter. This is indeed what happens, as it is shown in Figure 4.10, where we have represented the polarization and the current for four different values of γ.

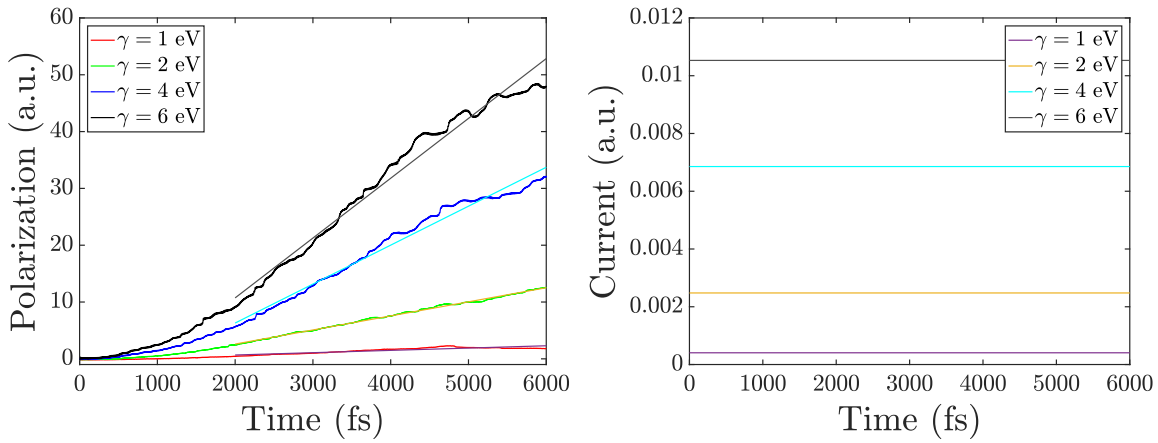

(a) (b)

Figure 4.10. Dependence of the current and the polarization of the linear chain on the band width. Note that the conductivity increases as the band width does.

Once we have seen the influence of γ in the conductivity of the system, let us reason the dependence on other parameters like the electron-lattice parameter or the force constant of the springs that represent the force field.

4.4.3.3. Dependence on the electron-lattice coupling

The electron-lattice coupling is a crucial part of the present work for the role it plays in the evolution from Bloch oscillations to ohmic transport. As it was mentioned in Section 3.5, this interaction can be characterized in terms of what we called the electron-lattice parameter, denoted as $\vec{f}$ and defined as in Eq.(3.53) and Eq.(3.54). Likewise, in Eq.(3.52) it was shown the effect of this electron-lattice interaction in the electronic part of the system, and so it is natural to ask what is the influence of the electron-lattice parameter on the transport properties in which we are interested. Intuitively, given that the lattice vibrations constitute one of the most relevant mechanisms of resistivity, we can expect that the greater the electron-lattice parameter, that is, the greater the electron-phonon coupling, the higher the resistivity and, thus, the lower the conductivity. More rigorously, from Eq.(3.52) it is easy to see that by increasing the value of the electron-lattice parameter, the term $\vec{f}_{\lambda\mu}\delta\vec{r}_{\lambda\mu}$ in γ becomes more important, that is, it increases

the electron-lattice coupling. This causes the variations in γ to be much wider, which results in a greater loss of periodicity; therefore, electrons will be more susceptible of being scattered by the lattice vibrations, giving rise to a higher electrical resistivity or, in other words, a lower conductivity. In order to verify these reasonings we carried out second-principles simulations for different values of the module $\vec{f}$ of the electron-lattice parameter. The results obtained are shown in Figure 4.11.

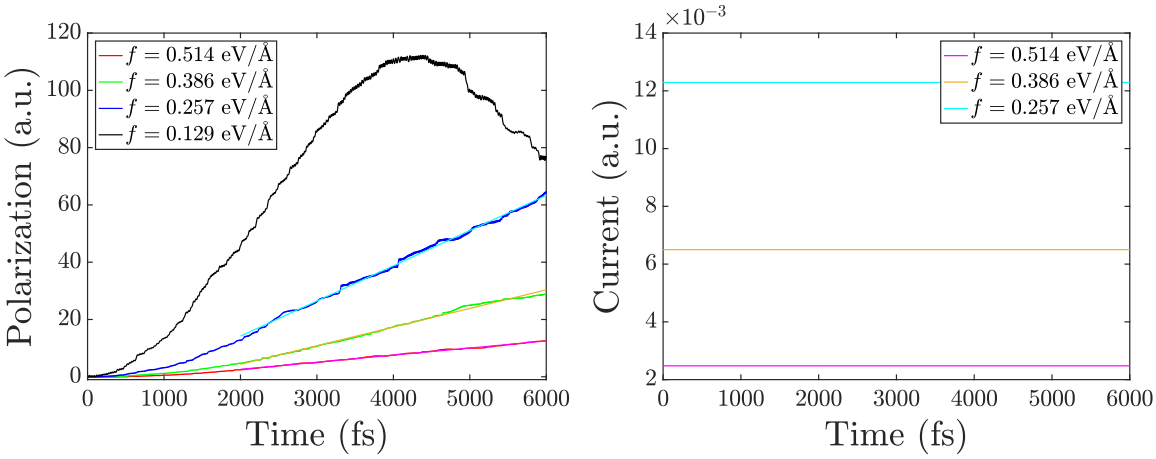

(a) (b)

FIGURE 4.11. Dependence of the current and the polarization of the linear chain on the electron-lattice coupling. In figure (a) we observe that when the electron-lattice coupling is small enough, Bloch oscillations dominate.

As it can be noted, the results obtained are the ones expected. However, it can be observed that for $f = 0.129\,\text{eV Å}^{-1}$, the polarization seems to present a trend to oscillate. This is due to the fact that the electron-lattice coupling is very small in that case and so we would be close to observing Bloch oscillations. Indeed, if we consider $f = 0$, what we obtain is precisely perfect Bloch oscillations, as it is shown in Figure 4.12. This is completely natural, since in that case the electrons do not feel the effect of the lattice vibrations.

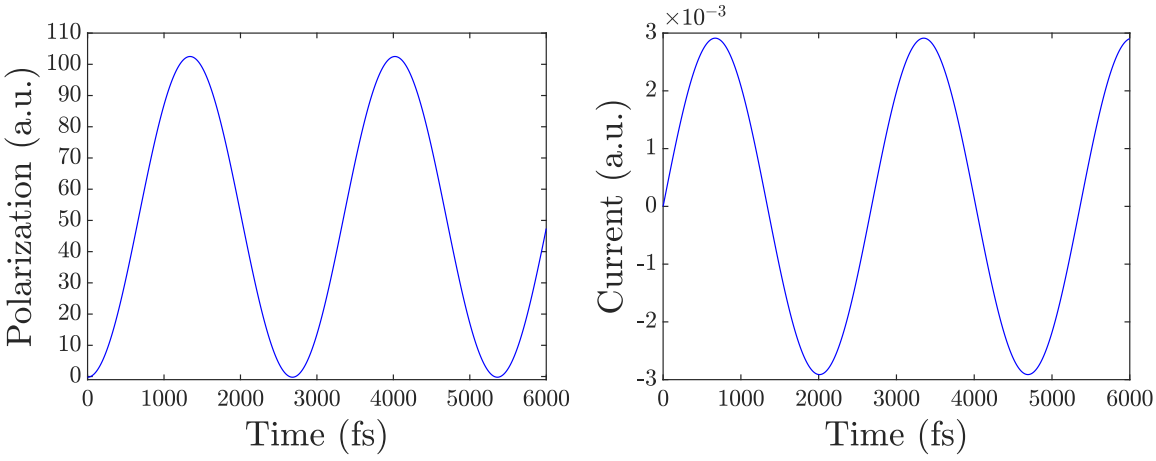

(a) (b)

FIGURE 4.12. Polarization and current of the linear chain when the electron-lattice parameter is $f = 0\,\text{eV Å}^{-1}$. We observe perfect Bloch oscillations, since in this case the electrons do not feel the effect of the vibrations.

4.4.3.4. Dependence on the phonon frequency

As it was mentioned in Section 3.5, to model the lattice vibrations we have employed a harmonic force field, so that atomic vibrations can be considered as movements of springs of force constant $\overleftrightarrow{K}$, a second-order tensor whose form is the one specified in Eq.(3.46). However, since we are considering interactions only in one direction, from now on we shall focus our attention on the longitudinal force constant K_σ, which will henceforth be denoted just as K for the sake of simplicity. As it is well known, the relation between this constant and the frequency of the oscillations of the springs is given by $\omega^2 = K/m$. Therefore, the frequency of the atomic vibrations, that is, the one of the phonons, is proportional to the force constant K. In order to study the dependence of the conductivity on the phonon frequency, in Figure 4.13 we show the results obtained for the current and the polarization for different values of the force constant K.

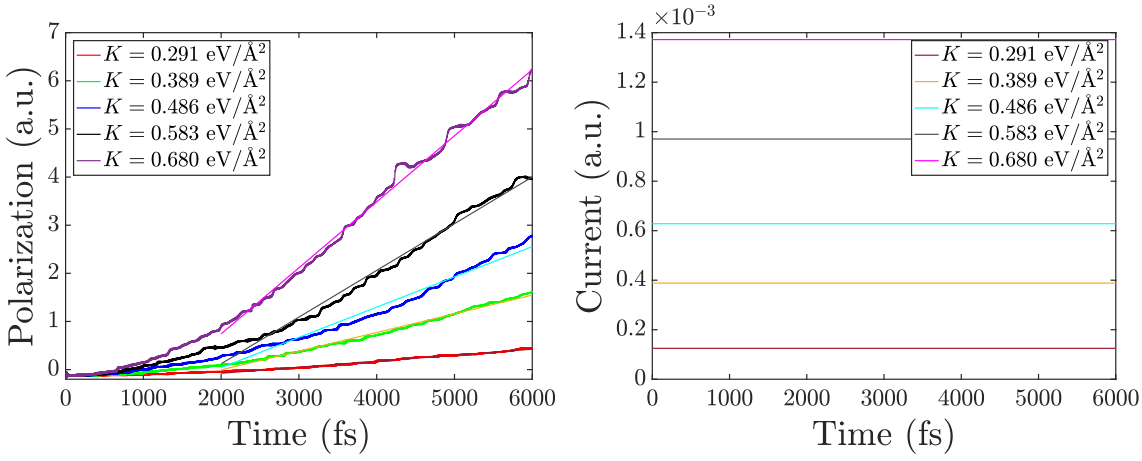

(a) (b)

Figure 4.13. Dependence of the polarization and the current of the linear chain on the phonon frequency. It can be appreciated that greater values of the force constant of the springs —and, therefore, of the phonon frequency— imply higher electrical conductivities.

As it can be appreciated in the previous figure, the conductivity increases as the phonon frequency does. The reason for this is that when we increase the value of the force constant K we are not modifying only the frequency of the vibrations but also their amplitude. To justify this affirmation, let us remember that under the harmonic approximation the vibrational energy of the system —considering only longitudinal movements— is given by:

$$E_\nu = \frac{1}{2} K Q_\nu^2 \,, \tag{4.12}$$

where Q_ν is a normal mode of the lattice. From the expression above it is easy to see that the vibrational energy is a parabola and that its curvature coincides with the force constant K. Moreover, given that we are considering a fixed temperature, we can visualize the vibrational energy as set to a fixed value $E \sim k_B T$, where k_B is the Boltzmann constant, and hence we are allowing only movements on the horizontal line of that energy, as it is schematically shown in Figure 4.14. It is clear from that figure that, for a fixed energy, greater values of K imply smaller amplitudes of the atomic movements. Therefore, taking into account Eq.(3.52) and applying the same reasoning that in the previous case, for a fixed electron-lattice parameter we shall have, from Eq.(3.52), smaller variations of γ and, therefore, a greater probability of resonance and thus a higher electrical conductivity. Hence, we conclude that the electrical conductivity is proportional to K, and thus to the phonon frequency, as we were trying to justify.

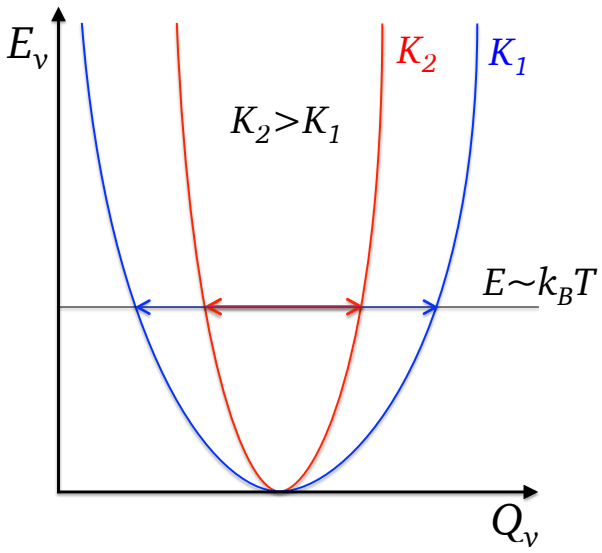

FIGURE 4.14. Schematic cartoon that illustrates the dependence of the amplitude of the atomic vibrations on the force constant K.

Here concludes the exposition and discussion of the principal results of this work. As a summary, after showing some results corresponding to the electronic and vibrational parts of the system, the role of the electron-lattice interaction in the translational symmetry breaking was illustrated through Peierls distortion. After that, we observed how Bloch oscillations arise at $T = 0\,\mathrm{K}$ and we provided with a simple two-level model that has helped us to better understand the origin of this phenomenon. Subsequently, by increasing the temperature it was checked that these oscillations are progressively distorted due to the atomic vibrations until reaching an ohmic regime at room temperature. Finally, through a systematic study of the conductivity at $T = 300\,\mathrm{K}$ we have showed the various trends of such magnitude with the amplitude of the electric field, the band width, the electron-lattice coupling and the phonon frequency.

CHAPTER 5

Conclusions

To finish this work, I would like to make some brief comments on the results obtained in relation to the objectives set at the beginning of this work and also on the future of the topic discussed in this dissertation.

In this work we have explored a topic that has so far received little discussion on textbooks due both to the difficulty that suppose a rigorous treatment of it and the absence of computational methods able to deal with systems of very many atoms or under conditions like finite temperatures or external fields. In this regard, the development of second-principles methods, implemented in the SCALE-UP tool, has given us the opportunity to make an initial exploration of very appealing phenomena like Bloch oscillations, the evolution from them to ohmic transport or the dependence of the electrical conductivity of solids on the parameters of the system, and all without resorting to any of the hypothesis of the semiclassical transport theory.

Hence, by considering a purely quantum one-dimensional tight-binding linear chain we have observed how Bloch oscillations emerge when a uniform static electric field is applied to a periodic system and it has been checked that the frequency of such oscillations varies with the amplitude of the applied electric field as predicted in the semiclassical model. To account for this, and also for the dependence of the amplitude of the oscillations on the electric field, we devised a simple two-level model that allows us to justify the observed Bloch oscillations by studying the temporal evolution of the occupation of each level for different values of the initial occupation.

Once the absolute zero case had been explored, it was checked the key role that the electron-lattice interaction plays in the evolution from Bloch oscillations to ohmic transport. More precisely, it was observed how this interaction causes the progressive distortion of the oscillations due to the loss of translational symmetry of the system. This was done through second-principles simulations carried out at intermediate temperatures between the absolute zero and the room temperature.

After that, a systematic study of the electrical conductivity at room temperature and its dependence on the applied electric field, the hopping parameter, the phonon frequency and the electron-lattice coupling was conducted, a study that has improved our understanding of the role that these parameters play on the transport properties of the system. It was observed that the electric current presents a dependence on the electric field which follows Ohm's law, but this dependence does not hold when we increase the electric field beyond a certain value. Moreover, if the amplitude of the electric field is large enough, the period of the Bloch oscillations becomes shorter than the relaxation time of the scattering of the electrons by the phonons, which allows us to observe such oscillations instead of the ohmic behaviour that we had for lower electric fields. Likewise, it is remarkable the dependence observed between the electrical conductivity and the band width, modified through the hopping parameter γ, as it has allowed us to justify the dependence on the phonon frequency —modified through the force constant K— and on the electron-lattice parameter f, since both dependencies lie on the electron-lattice coupling term in γ.

Finally, regarding the future of the topics covered in this dissertation, it is clear that the natural extension of this work is the study of transport phenomena, especially of electrical conductivity in solids, in real physical systems rather than in simple models, which will allow us to contrast the results obtained with the known experimental data. For this purpose, it will be necessary to use the second-principles techniques already described, with the difference that, in the case of real systems, the parameters will have to be obtained through rigorous first-principles calculations.

In addition, this work could also be extended, at a more advanced level, to some exciting topics that will probably be of great relevance in the near future, like superconductivity, transport in solids and interfaces, metal-insulator transitions, spintronics or thermoelectricity and heat transport. Hence, it is undeniable that scientific research in this field has a promising future that will be certainly marked by the progressive development and improvement of the second-principles techniques and similar approaches, which will take the research in condensed matter theory to a new and deeper level of comprehension.

References

[1] J. M. Ziman. *Electrons and Phonons: The Theory of Transport Phenomena in Solids.* Oxford University Press, 2003.

[2] D. R. Lide. *CRC Handbook of Chemistry and Physics.* CRC Press, 85th edition, 2005.

[3] P. Hofmann. *Solid State Physics: An Introduction.* Wiley-VCH, 2nd edition, 2015.

[4] R. K. Wangsness. *Electromagnetic Fields.* John Wiley & Sons, 2nd edition, 1986.

[5] C. Cohen-Tannoudji, B. Diu, F. Lalo. *Quantum Mechanics.* Wiley, 1977.

[6] P. Drude. *Zur Elektronentheorie der Metalle.* Annalen der Physik, 306(3), 1900.

[7] E. Eser, H. Koç. *Investigations of temperature dependences of electrical resistivity and specific heat capacity of metals.* Physica B: Condensed Matter, 492, 2016.

[8] F. Giustino. *Electron-phonon interactions from first principles.* Rev. Mod. Phys., 89(015003), 2017.

[9] F. Bloch. *Über die Quantenmechanik der Elektronen in Kristallgittern.* Zeitschrift für Physik, 52 (7-8), 1928.

[10] N. W. Ashcroft, N. D. Mermin. *Solid State Physics.* Harcourt College Publishers, 1976.

[11] G. H. Wannier. *Wave Functions and Effective Hamiltonian for Bloch Electrons in an Electric Field.* Phys. Rev., 117(2), 1960.

[12] I. Souza, J. Íñiguez, D. Vanderbilt. *Dynamics of Berry-phase polarization in time-dependent electric fields.* Phys. Rev. B, 69(085106), 2004.

[13] C. Zener. *A theory of the electrical breakdown of solid dielectrics.* Proc. R. Soc. A, 145(855), 1934.

[14] H. Ibach, H. Lüth. *Solid-State Physics.* Springer, 2nd edition, 1996.

[15] L. Esaki and R. Tsu. *Superlattice and Negative Differential Conductivity in Semiconductors.* IBM J. Res. Develop, 14(1), 1970.

[16] J. Feldmann et al. *Optical investigation of Bloch oscillations in a semiconductor superlattice.* Phys. Rev. B, 46(7252(R)), 1992.

[17] P. W. Atkins and R. S. Friedman. *Molecular Quantum Mechanics.* Oxford University Press, 4th edition, 2005.

[18] F. Jensen. *Introduction to Computational Chemistry.* John Wiley & Sons, 1999.

[19] P. Hohenberg, W. Kohn. *Inhomogeneous Electron Gas.* Phys. Rev., 136(B864), 1964.

[20] W. Kohn, L. J. Sham. *Self-Consistent Equations Including Exchange and Correlation Effects.* Phys. Rev., 140(A1133), 1965.

[21] E. Runge, E. K. U. Gross. *Density-Functional Theory for Time-Dependent Systems.* Phys. Rev. Lett., 52(997), 1984.

[22] E. K. U. Gross, W. Kohn. *Local density-functional theory of frequency-dependent linear response.* Phys. Rev. Lett., 55(2850), 1985.

[23] M. Petersilka, U. J. Grossman, E. K. U. Gross. *Excitation Energies from Time-Dependent Density-Functional Theory.* Phys. Rev. Lett, 76(1212), 1996.

[24] P. García-Fernandez, J. Wojdeł, J. Íñiguez, J. Junquera. *Second-principles method for materials simulation including electron and lattice degrees of freedom.* Phys. Rev. B, 93(195137), 2016.

[25] R. Parr, W. Yang. *Density-Functional Theory of Atoms and Molecules*. Oxford University Press, 1994.

[26] P. García-Fernandez, J. Íñiguez, J. Junquera. *Extension of Second-Principles Density Functional Theory into the time domain*. Unpublished manuscript.

[27] D. Vanderbilt, R. D. King-Smith. *Electric polarization as a bulk quantity and its relation to surface charge*. Phys. Rev. B, 48(4442), 1993.

[28] R. Resta, D. Vanderbilt. *Theory of Polarization: A Modern Approach*, volume 105, pages 31–68. 2007.

[29] E. Kaxiras. *Atomic and Electronic Structure of Solids*. Cambridge University Press, 2003.

[30] S. H. Simon. *Lecture Notes for Solid State Physics*. 2012.

[31] M. T. Dove. *Structure and Dynamics: An atomic view of materials*. Oxford University Press, 2003.

[32] W. A. Harrison. *Solid State Theory*. Dover Publications, 2nd edition, 1979.

[33] scale-up software package. https://www.secondprinciples.unican.es/, 2017.

[34] R. E. Peierls. *Quantum theory of Solids*. Oxford University Press, 1955.